Investigation of Unbraced Pile Height in Fully Encased Pile Bents of Bridge Structures

Final Report
May 2026

BRIDGE ENGINEERING CENTER

IOWA STATE UNIVERSITY
Institute for Transportation

Sponsored by
Iowa Department of Transportation
and Federal Highway Administration
(SPR-RE23(008)–8H-00,
InTrans Project 22-827)

About the Bridge Engineering Center

The mission of the Bridge Engineering Center (BEC) is to conduct research on bridge technologies to help bridge designers/owners design, build, and maintain long-lasting bridges.

About the Institute for Transportation

The mission of the Institute for Transportation (InTrans) at Iowa State University is to save lives and improve economic vitality through discovery, research innovation, outreach, and the implementation of bold ideas.

Iowa State University Nondiscrimination Statement

Iowa State University does not discriminate on the basis of race, color, age, ethnicity, religion, national origin, pregnancy, sexual orientation, genetic information, sex, marital status, disability, or status as a U.S. Veteran. Inquiries regarding nondiscrimination policies may be directed to Office of Equal Opportunity, 2680 Beardshear Hall, 515 Morrill Road, Ames, Iowa 50011, telephone: 515-294-7612, email: eooffice@iastate.edu.

Disclaimer Notice

The contents of this report reflect the views of the authors, who are responsible for the facts and the accuracy of the information presented herein. The opinions, findings and conclusions expressed in this publication are those of the authors and not necessarily those of the sponsors.

The sponsors assume no liability for the contents or use of the information contained in this document. This report does not constitute a standard, specification, or regulation.

The sponsors do not endorse products or manufacturers. Trademarks or manufacturers' names appear in this report only because they are considered essential to the objective of the document.

Quality Assurance Statement

The Federal Highway Administration (FHWA) provides high-quality information to serve Government, industry, and the public in a manner that promotes public understanding. Standards and policies are used to ensure and maximize the quality, objectivity, utility, and integrity of its information. The FHWA periodically reviews quality issues and adjusts its programs and processes to ensure continuous quality improvement.

Iowa DOT Statements

The Iowa Department of Transportation (DOT) ensures non-discrimination in all programs and activities in accordance with Title VI of the Civil Rights Act of 1964. Any person who believes that they are being denied participation in a project, being denied benefits of a program, or otherwise being discriminated against because of race, color, national origin, gender, age, or disability, low income and limited English proficiency, or if needs more information or special assistance for persons with disabilities or limited English proficiency, please contact Iowa DOT Civil Rights at 515-239-7970 or by email at civil.rights@iowadot.us.

The preparation of this report was financed in part through funds provided by the Iowa DOT through its "Second Revised Agreement for Management of Research Conducted by Iowa State University for the Iowa Department of Transportation" and its amendments.

The opinions, findings, and conclusions expressed in this publication are those of the authors and not necessarily those of the Iowa DOT or the U.S. DOT.

Technical Report Documentation Page

1. Report No.	2. Government Accession No.	3. Recipient's Catalog No.
InTrans Project 22-827		

4. Title and Subtitle	5. Report Date
Investigation of Unbraced Pile Height in Fully Encased Pile Bents of Bridge Structures	May 2026
	6. Performing Organization Code

7. Author(s)	8. Performing Organization Report No.
Justin Dahlberg (orcid.org/0000-0002-6184-4122), Zhengyu Liu (orcid.org/0000-0002-7407-0912), Abdalla Alomari (orcid.org/0000-0002-0995-2599), Zachary Kahle	InTrans Project 22-827

9. Performing Organization Name and Address	10. Work Unit No. (TRAIS)
Bridge Engineering Center Iowa State University 2711 South Loop Drive, Suite 4700 Ames, IA 50010-8664	**11. Contract or Grant No.**

12. Sponsoring Organization Name and Address		13. Type of Report and Period Covered
Iowa Department of Transportation 800 Lincoln Way Ames, IA 50010	Federal Highway Administration 1200 New Jersey Avenue, SE Washington, DC 20590	Final Report
		14. Sponsoring Agency Code SPR-RE23(008)–8H-00

15. Supplementary Notes

Visit https://bec.iastate.edu/ for color pdfs of this and other research reports.

16. Abstract

This study investigated the structural performance of fully encased steel H-piles used in bridge foundations, with a specific focus on the effects of unbraced pile height resulting from scour conditions. While concrete encasement is widely used to protect piles, its structural contribution is often excluded from axial capacity calculations in current design practice. This research aimed to evaluate the effectiveness of fully encased pile bents in enhancing pile stability and to refine an existing assessment tool for more accurate capacity estimations.

The project combined full-scale laboratory testing and finite element (FE) modeling. Two major tests were performed: a three-pile fully encased bent subjected to service-level loads and a single encased pile tested to failure. Results showed increased stiffness, increased load-sharing behavior, and a significant gain in axial capacity due to encasement.

Validated FE models were used to conduct parametric studies assessing the effects of encasement length, pile length, and axis orientation. Findings confirmed that full encasement and weak-axis restraint significantly improve axial performance.

This research supports the inclusion of concrete encasement in pile capacity evaluations and provides engineers with a validated tool for more resilient and cost-effective bridge foundation design.

17. Key Words	18. Distribution Statement
bridge foundations—concrete encasement—pile bents—steel H-piles	No restrictions.

19. Security Classification (of this report)	20. Security Classification (of this page)	21. No. of Pages	22. Price
Unclassified.	Unclassified.	93	NA

Form DOT F 1700.7 (8-72) **Reproduction of completed page authorized**

INVESTIGATION OF UNBRACED PILE HEIGHT IN FULLY ENCASED PILE BENTS OF BRIDGE STRUCTURES

Final Report
May 2026

Principal Investigator
Justin Dahlberg, Director
Bridge Engineer Center, Iowa State University

Co-Principal Investigator(s)
Brent M. Phares, Research Engineer
Bridge Engineer Center, Iowa State University

Authors
Justin Dahlberg, Zhengyu Liu, Abdalla Alomari, and Zachary Kahle

Sponsored by
Iowa Department of Transportation
(SPR-RE23(008)–8H-00)

Preparation of this report was financed in part
through funds provided by the Iowa Department of Transportation
through its Research Management Agreement with the
Institute for Transportation
(InTrans Project 22-827)

A report from
Bridge Engineering Center
Iowa State University
2711 South Loop Drive, Suite 4700
Ames, IA 50010-8664
Phone: 515-294-8103 / Fax: 515-294-0467
https://bec.iastate.edu/

TABLE OF CONTENTS

LIST OF FIGURES

LIST OF TABLES

ACKNOWLEDGMENTS

The research team would like to acknowledge the Iowa Department of Transportation (Iowa DOT) for sponsoring this research and the Federal Highway Administration (FHWA) for the state planning and research (SPR) funds used for this project. Special thanks are extended to Mike Nop, Jim Denny, Jim Hauber, and Shawn Sersland of the Iowa DOT for their guidance and service on the project oversight committee. The team also wishes to recognize Owen Steffens and the staff of the Structural Laboratory at Iowa State University for their assistance and contributions to the successful completion of the laboratory testing.

EXECUTIVE SUMMARY

Steel H-piles are commonly used in bridge foundations throughout Iowa, often with concrete encasement to protect against corrosion and mechanical damage. However, current design practices do not account for the structural contribution of this encasement, particularly in cases where scour reduces the surrounding soil support. This conservative assumption can result in overdesigned systems and missed opportunities for cost savings.

This study investigated the axial capacity and stability of fully encased H-piles under conditions simulating scour-induced unbraced heights. The research aimed to evaluate the structural performance of fully encased pile bents compared to individually encased ones and to enhance previously conducted work estimating pile capacity under such conditions.

A comprehensive approach was undertaken, including a literature review, full-scale laboratory testing, and finite element (FE) modeling. Laboratory tests included a three-pile fully encased assembly tested under service loads and a single-pile assembly tested to failure. Results showed that encasement significantly enhances stiffness and load capacity, with the single-pile assembly achieving a peak capacity of 668 kips—about 18% more than that of similar configurations using Iowa's standard P10L encasement.

FE models were validated against test data and used to explore the effects of pile length, encasement length, and pile orientation. The results confirmed that longer encasement lengths and weak-axis restraint configurations provide significantly higher capacities. Fully encased piles consistently outperformed their singly encased counterparts.

The updated pile capacity calculations presented in this report include full encasement options and yield conservative but more accurate estimations than standard methods. These findings support revisions to design practices, particularly for scour-prone areas, offering improved safety, structural performance, and potential cost reductions in bridge design.

This research bridges gaps in current practice by validating the structural benefits of encasement and equipping engineers with better tools for resilient, efficient bridge foundation design.

1 INTRODUCTION

1.1 Background

The current standard design of steel H-pile bents in Iowa does not include the capacity contribution of the concrete encasement that is used for protection against corrosion and other damaging effects. This has become a notable issue when pile bents are subjected to scour events and a load rating engineer is left to determine the actual capacity of the piles.

For this reason, a project recently completed for the Iowa Department of Transportation (Iowa DOT) investigated the contributions of standard P10L concrete encasements of steel H-piles used for bridges, which have historically not been considered in the design process (Deng et al. 2018). The primary reason for the project was to determine the remaining capacity of a pile when subjected to scour, which leaves bare the unencased portion of a pile. A rapid assessment tool was developed to calculate the capacities of individual concrete-encased piles. The assessment tool estimated capacities for encased piles that were greater than the calculated capacities of unencased piles. To further validate the capabilities of the assessment tool, a laboratory investigation was completed, which provided results for four different pile encasement variations (Liu et al. 2021a). The specimens were tested in a pin-fixed boundary condition without any eccentricity. The results from the experimental tests were compared with the estimations from the assessment tool. The key findings included the following:

- The pile assessment tool provides a conservative estimation of the axial capacity of the piles. The estimation results were 8% to 24% lower than those from the experimental results.
- Concrete encasement increases the initial axial stiffness of the piles.
- Consideration of the concrete encasement greatly increases the axial capacity of the piles.
- Ignoring the effect of the concrete encasement, as with the use of the equations suggested by the American Institute of Steel Construction (AISC), can result in a significantly conservative estimation.
- As a result, consideration has been given to include the concrete encasement contribution to newly designed piles in addition to providing a tool to evaluate existing piles.

As a secondary result, consideration was given to revising the capacity calculations of new piles, especially in fully encased pile bents. For new bridge designs, it has been found more cost-effective to fully encase a grouping of pier piles in a single concrete pier than to individually encase each pile. See Figure 1-1. Currently, the decision to fully encase rather than individually encase piles is made when there are ice or debris issues associated with the waterway in which the pier stands. Determining that the unbraced height of fully encased piles meets or exceeds the unbraced height of individually encased piles would allow for more fully encased pile bents to be constructed, resulting in cost savings for bridge projects.

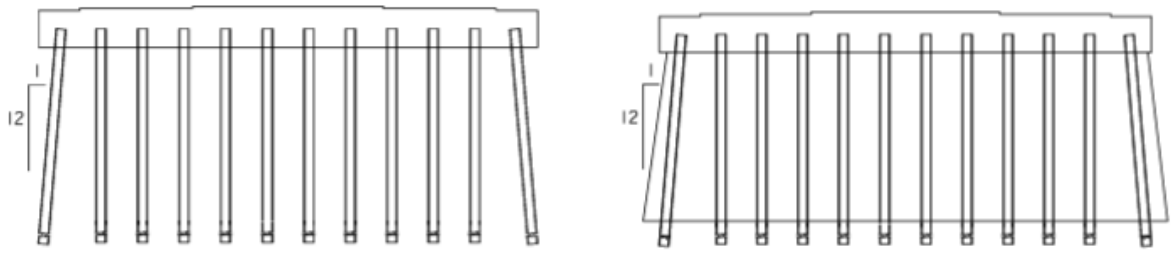

Figure 1-1. Pile bent with individually encased piles (left) and fully encased piles (right)

1.2 Problem Statement

Fully encased pile bents are used for bridges in the state of Iowa with regularity. It is believed that the unbraced height limits of these pile bents may be greater than the limits of individually encased piles when subjected to the same axial load. In situations where greater amounts of scour are observed, this may alleviate immediate capacity concerns.

The current practice of designing a fully encased pile bent in Iowa is to place the weak axis of the pile parallel to the bridge longitudinal direction, with the exterior piles battered at a 1:12 slope. Reviewing the standard orientation may reveal that additional efficiencies can be realized by changing the pile orientation.

1.3 Objective and Approach

The objective of this project was to identify the maximum unbraced height of fully encased piles and to further develop the capacity calculations initially developed in previous research to include fully encased options.

1.4 Research Plan and Deliverables

The objectives of this project were achieved via the following primary tasks:

1. Literature review
2. Laboratory investigation of the capacity of multiple and single piles in fully encased configurations
3. Analytical simulation to estimate pile capacities

The results of this research included validated capacity calculations that inform design and load rating engineers regarding the capacity of fully encased H-piles, providing additional information for bridge substructure design and assessment.

2 LITERATURE REVIEW

The main objective of this task was to obtain a greater understanding of the behavior of concrete-encased steel H-piles used for bridge projects. As part of this task, a literature review on concrete encased piles was conducted. Further, the current state of the practice on the use of fully encased piles was reviewed, and information was gathered on the performance of previously constructed bridges in Iowa in which fully encased pile bents were used.

2.1 Bridge Concrete Encased Pile Foundation

A driven pile foundation is one of several deep foundation types that are commonly used in the United States for highway bridges. Steel H-piles are one of the conventional types of piles in this foundation system. Typically, these piles are rolled wide-flange structural sections with flange widths approximately equal to the section depth. Similar to other piles, H-piles can achieve their nominal axial resistance through shaft (friction) resistance, toe (bearing) resistance, or a combination of both. Early studies in 1964 on full-scale 13 in. diameter timber piles with a 52 ft unsupported length above the ground revealed that buckling is the main failure mechanism of bridge foundation piles (Klohn and Hughes 1964). Various studies were conducted investigating the buckling behavior of partially and fully embedded piles from various perspectives. Early studies on this topic resulted in p-y curves developed by McCelland and Focht in 1958 based on the theory of beams on an elastic foundation developed by Winkler in 1867 (McClelland and Focht Jr 1958, Khodair and Abdel-Mohti 2014). Later, many studies were conducted to investigate the effects of soil-pile interactions on the buckling failure of piles. Further analyses of the soil-pile interaction revealed that piles can be considered completely fixed at approximately 5 ft below the ground line unless the soil modulus (k_0) is very small, i.e., $k_0 < 5$ lb/in^3 (Vogt et al. 2009, Hughes et al. 1998).

The axial capacities of piles are highly dependent on the surrounding soil conditions. Scour, defined as “the erosion or removal of a streambed or bank material from bridge foundations due to flowing water” (Kattell and Eriksson 1998), reduces the presence of soil surrounding the piles and results in an increased unbraced length, which negatively impacts the capacity and stability of the piles. According to a study in 2007, 60% of bridge failures in the United States are caused by scour (Lagasse et al. 2007, Liang et al. 2007). There have been various studies conducted regarding the effect of scour on the buckling failure of pile foundations. An integrated analysis of scour was conducted in a previous study that considered nonlinear water-soil-structure interactions and the interactions between substructure and superstructure (Lin et al. 2012). It was revealed that integrated techniques provide accurate results without making oversimplifying assumptions. Extreme scour can also change the undrained shear strength of the remaining soil, and this can affect the lateral subgrade modulus of the soil. This issue can lead to a reduction of 12% to 14% of the buckling load of the pile during extreme scour conditions (Liang et al. 2015).

Corrosion is another phenomenon that can reduce pile capacity or even lead to failure by reduction of the pile’s cross-sectional area. The presence of oxygen is required for corrosion to occur, and, fortunately, at deeper levels, corrosion has not been a pervasive issue due to the relatively quick consumption of the limited amount of oxygen in soils or the absence of oxygen

altogether (Hannigan et al. 1998). At higher levels or at grade, concrete encasement has been commonly used to protect bridge piles from corrosion where they are exposed to air and water. This encasement protects the bare steel pile against repetitive wet-dry cycles induced by changing river water levels. Although there is no common requirement for concrete encasement in nationwide design codes, states have developed their own concrete encasement details. In this approach, a certain length of the pile is encased with concrete, while the remaining portion of the pile is not.

Previous experimental research was performed on fully encased steel piles to investigate the buckling capacity of these composite members (Rahman et al. 2016, El-Barbary et al. 2011); however, little research was found that investigated the buckling behavior of partially encased piles. Recently, research was conducted to investigate the efficiency of concrete encasement (also named jacketing) in improving the capacity of piles after corrosion occurs. These studies revealed that using conventional concrete, fiber-reinforced plastic (FRP), or carbon fiber-reinforced plastic (CFRP) jacketing systems in a limited locally corroded length of a pile can efficiently restore the capacity of the pile to its nominal design capacity (Liu et al. 2005, Vijay et al. 2016, Dawood et al. 2017, Karagah et al. 2018, Abdulazeez et al. 2019).

In the state of Iowa, concrete encasement is used before the occurrence of corrosion (Iowa DOT 2021). In the LRFD Trestle Pile Bent standard developed by the Iowa DOT (Iowa DOT 2019), concrete encasement around the pile begins at the pile cap, covers all of the exposed length of the pile, and extends 3 ft below the stream bed or ground level. Figure 2-1 (a) shows a schematic view of a pile with concrete encasement. Based on this standard, concrete encasement could be square or round in shape, with final dimensions dependent on the steel pile size. However, the effect of the concrete encasement on the axial pile capacity is ignored during the design stage because it is assumed that there is no positive shear connection between the steel pile and concrete encasement (Iowa DOT 2009). Although concrete encasement does not extend the whole length of a pile, it affects the cross-sectional properties of the pile where encasement exists (Deng et al. 2018, Liu et al. 2021a). This is an important consideration in situations of scour, as shown in Figure 2-1 (b), where rating engineers need to make a more accurate estimation of axial pile capacity.

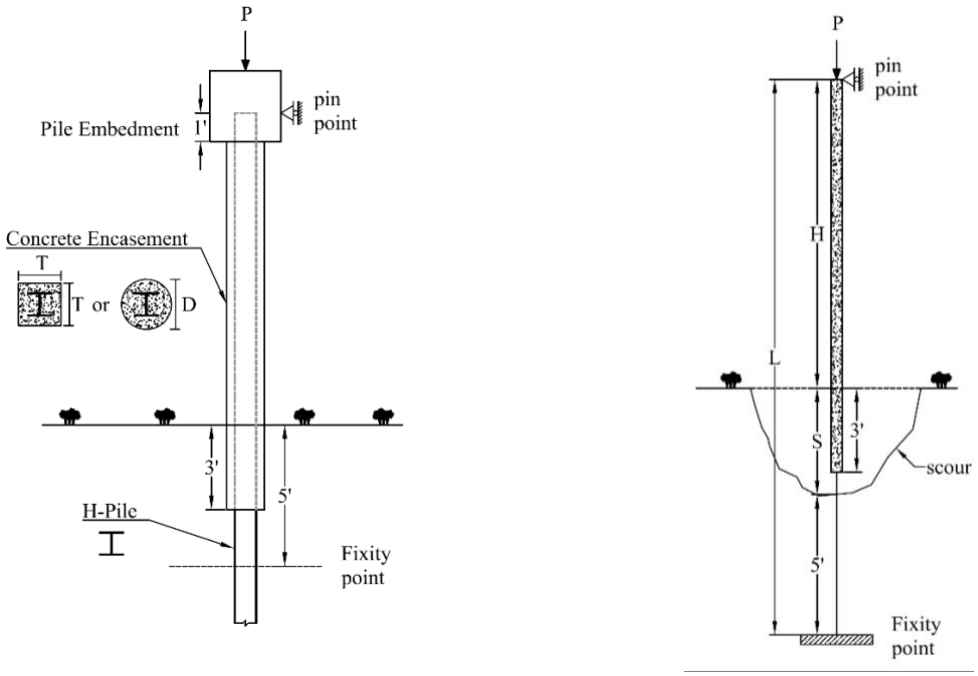

(a) Steel H-pile with concrete encasement

(b) Pile in scour situation.

Figure 2-1. Schematic view of a pile foundation with concrete encasement and in a scour situation

To help rating engineers provide timely, realistic estimations of pile capacity, Deng et al. (2018) developed an assessment tool to quickly determine pile capacity. The tool takes into account both the unbraced pile lengths and the stiffness contribution of concrete encasements. A numerical evaluation program was developed and implemented to offer a user-friendly assessment tool that can be used to quickly evaluate pile strength. The numerical program consisted of finite element (FE) models established for steel H-piles with or without concrete encasement and with consideration of linear and nonlinear buckling and behavior. The FE models were validated against capacities calculated based on the provisions outlined in the AISC *Steel Construction Manual* (AISC 2017). After that, a parametric study was conducted to understand the influence of concrete encasements on pile buckling strength. Various combinations of unbraced pile lengths and concrete encasement lengths were investigated. The relationships between the buckling strength of steel H-piles with concrete encasements under concentric and eccentric loading conditions were derived from the results of the parametric studies. For the user's convenience, the researchers developed a graphical user interface for the tool, which requires the user to input four parameters: loading eccentricity, H-pile section type, unbraced pile length, and concrete encasement length. This pile assessment tool can be utilized to quickly calculate pile capacity and assist state rating engineers in making rapid decisions regarding pile capacity. However, this rapid pile assessment tool was developed and verified using provisions and theoretical modeling approaches. Experimental data to validate the tool's results were not available as part of that study.

Liu et al. (2021a) conducted a series of experiments to validate the previously developed rapid pile assessment tool's findings to ensure accurate pile capacity determination, both for bare piles

and those encased in concrete. To achieve this goal, four specimens with various lengths and concrete encasement lengths and ratios were constructed and tested via axial loading in the laboratory. All specimens were HP10×42 cross-sections (with various lengths). The first and second specimens were 16 ft long, while the third and fourth specimens were 30 ft and 38 ft long, respectively. The first specimen had no concrete encasement, and the lengths of encasement for the second, third, and fourth specimens were 10, 20, and 30 ft, respectively. The specimens were tested in a pin-fixed boundary condition without any eccentricity. In summary, the previously developed pile capacity assessment tool was validated through the experimental results and was confirmed to provide a conservative estimation of pile capacity for concrete-encased piles. While providing conservative results, the capacities resulting from the tool were found to be significantly higher than those obtained using AISC specifications. As such, valuable additional capacity can be realized when including the contribution from concrete encasements.

2.2 Analytical Solution for the Buckling Load of Partially Encased Steel H-piles

The first study on the stability of elastic compression members is attributed to Leonhard Euler in the 18th century, who obtained an equilibrium equation and derived buckling load using the theory of calculus (Timoshenko and Gere 2009). Based on this work, the elastic buckling capacity of a compression member can be calculated utilizing equation (1).

$$P = \frac{\pi^2 EI}{(KL)^2} \tag{1}$$

where P is the elastic buckling force, E is the elastic modulus, I is the moment of inertia of the section, L is the length of the member, and K is the effective length coefficient dependent on the boundary condition of the compression member.

For bridge piles, a fixed condition can be assumed at approximately 5 ft below the ground level (Hughes et al. 2007), and the upper end of the pile can be assumed to be pin-supported. Figure 2-2 (a) shows a schematic view of a pile and its assumed boundary conditions. The effective length coefficient (K) for a compression member with a uniform cross-section and a pin-fixed condition is 0.7 (ASTM A572).

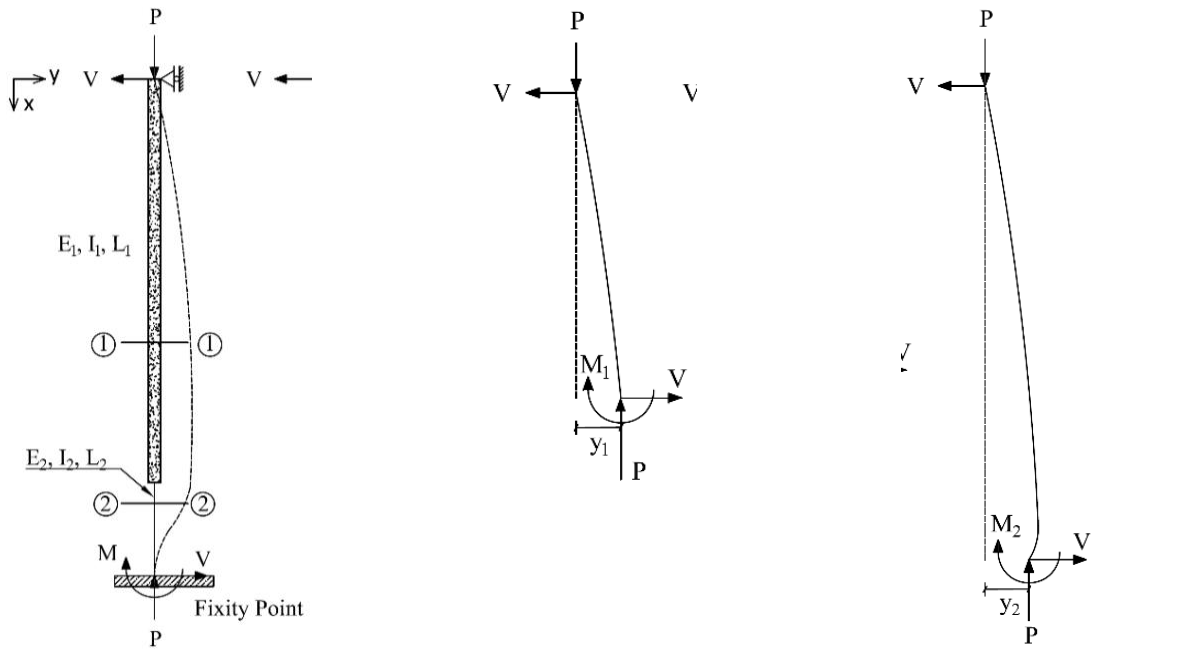

(a) Boundary conditions and pile properties

(b) Equilibrium in the encased portion

(c) Equilibrium in the bare steel portion

Figure 2-2. Schematic view of a pile foundation and assumed boundary conditions

However, for members such as encased piles with two different cross-sections along the pile, this coefficient (K) varies with the length, cross-section, and material properties of the concrete encasement. Mousavi et al. (2022) developed an analytical solution for the estimation of the capacities of encased piles. Figure 2-2 (b) and Figure 2-2 (c) show the forces and moments in Sections 1-1 and 2-2 of Figure 2-2 (a), respectively. The moment equilibrium for Section 1-1 and Section 2-2 can be expressed utilizing equation (2) and equation (3).

$$M_1 + Vx = Py_1 \tag{2}$$

$$M_2 + Vx = Py_2 \tag{3}$$

The internal moment in Sections 1-1 and 2-2 can be expressed utilizing equations (4) and (5), respectively.

$$M_1 = -E_1 I_1 y_1^{"} \tag{4}$$

$$M_2 = -E_2 I_2 y_2^{"} \tag{5}$$

Substituting M_1 and M_2 in equation (2) and equation (3) by equation (4) and equation (5), respectively, the following equations can be achieved.

$$y_1^{"} + K_1^2 y_1 - \frac{M}{E_1 I_1 L} x = 0 \tag{6}$$

$$y_2^{"} + K_2^2 y_2 - \frac{M}{E_2 I_2 L} x = 0 \tag{7}$$

where,

$$L = L_1 + L_2 \tag{8}$$

$$K_1^2 = \frac{P}{E_1 I_1} \quad , \quad K_2^2 = \frac{P}{E_2 I_2} \tag{9}$$

The general solutions for equation (6) and equation (7) are as shown in equations (10) and (11).

$$y_1 = A \sin(k_1 x) + B \cos(k_1 x) + \frac{M}{PL} x \tag{10}$$

$$y_2 = C \sin(k_2 x) + D \cos(k_2 x) + \frac{M}{PL} x \tag{11}$$

The boundary conditions and continuity conditions can be expressed as follows:

Boundary conditions:
$$\begin{cases} y_1(x = 0) = 0 & \text{(I)} \\ y_2(x = L) = 0 & \text{(II)} \\ \frac{dy_2}{dx}(x = L) = 0 & \text{(III)} \end{cases}$$

Continuity conditions:
$$\begin{cases} y_1(x = L_1) = y_2(x = L_1) & \text{(IV)} \\ \frac{dy_1}{dx}(x = L_1) = \frac{dy_2}{dx}(x = L_1) & \text{(V)} \end{cases}$$

With the general solutions, boundary conditions, and continuity equation, the following solution can be achieved:

$$\frac{K_2 L - \tan(K_2 L)}{1 + K_2 L \tan(K_2 L)} = \frac{\tan(K_1 L_1) - \frac{K_1}{K_2}\tan(K_2 L_1)}{\tan(K_1 L_1)\tan(K_2 L_1) + \frac{K_1}{K_2}} \tag{12}$$

If the pile has a uniform cross-section and no concrete encasement, K_1 equals K_2, and equation (12) turns into KL = tan (KL), which is the solution for a compression member with a pin-fixed

condition with K equal to 0.7 (Timoshenko and Gere 2009). In order to solve equation (12) for a nonuniform cross-section, equation (12) can be rearranged as equation (13) by defining unitless values of α, β, and m:

$$\frac{(\alpha\beta m)-\tan(\alpha\beta m)}{1+(\alpha\beta m)\tan(\alpha\beta m)} = \frac{\tan(m)-(1/\alpha)\tan(\alpha m)}{\tan(m)\tan(\alpha m)+(1/\alpha)} \quad (13)$$

where,

$$\alpha = \frac{K_2}{K_1} = \sqrt{\frac{E_1 I_1}{E_2 I_2}} \quad (14)$$

$$\beta = \frac{L}{L_1} \quad (15)$$

$$K_2 L = \alpha\beta m \quad (16)$$

In the above equation, α is the ratio of k_2 and k_1, which is equal to the square root of the ratio of $E_1 I_1$ and $E_2 I_2$, and β value is the ratio of the total length to the encased length. Both α and β depend on material properties and geometries. The only unknown variable in equation (13) is *m*. Once equation (13) is solved and *m* is determined, it can be used with equation (16) and equation (9) to determine the elastic buckling force as follows:

$$P = \frac{\alpha^2\beta^2 m^2 E_2 I_2}{L^2} \quad (17)$$

The above equation can be rewritten as follows:

$$P = \frac{\pi^2 E_2 I_2}{(K'L)^2} \quad (18)$$

where K' is a modified effective length coefficient and can be calculated as follows:

$$K' = \frac{\pi}{\alpha\beta m} \quad (19)$$

Equation (19) indicates that when part of a pile is encased by concrete, the effective length not only depends on the boundary condition but also on α, the square root of the flexural stiffness ratio, and β, the ratio of the pile length to the concrete encasement length.

2.3 Use of Fully Encased Pile Encasement

Pile bents with fully encased piles have been used by multiple state departments of transportation (DOTs) in the United States. For example, in Iowa, pile bents are the usual selection for low-

level, short-span continuous concrete slab (CCS), pretensioned prestressed concrete beam (PPCB), or rolled steel beam (RSB) bridges (Iowa DOT 2023). For stream or river crossings with ice or driftwood flows that are expected to cause lateral loading of the bridge piers, the pile bent is fully encased. End piles are battered at a slope of 1:12, as shown in Figure 2-3. Superstructure spans exceeding 100 ft usually require pile bents with excessive numbers of piles, and for longer spans, T-piers or frame piers are a better choice. Pile bents are appropriate for stream and river crossings with drainage areas less than 50 mi^2.

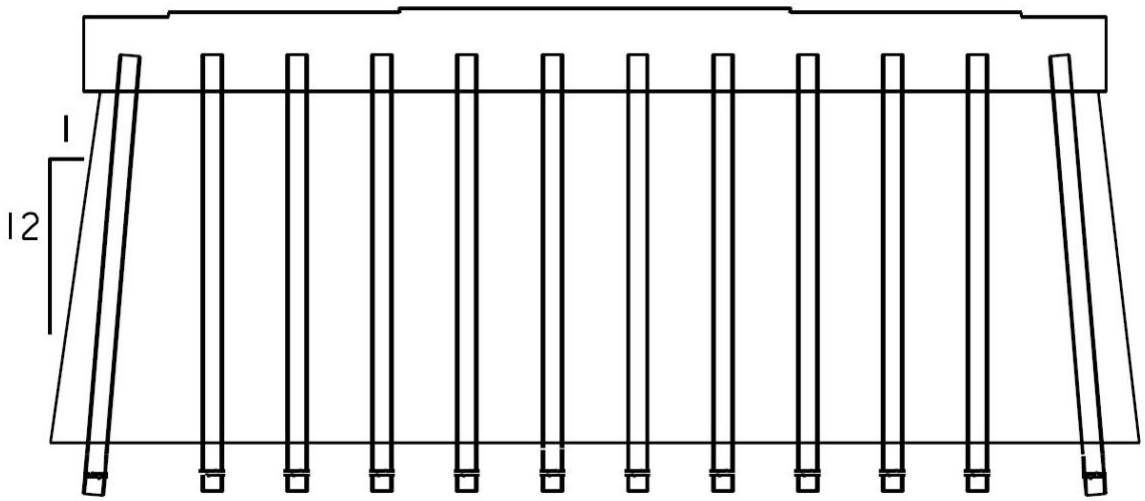

Iowa DOT 2023

Figure 2-3. Pile bent with fully encased piles

The Minnesota Department of Transportation (MnDOT) lists the advantages and disadvantages of encased pile bent piers (MnDOT 2023). The advantages include the following:

- Encased pile bent piers are generally lower cost and easier to construct than footing-supported pier structures.
- Encasement walls can be built with aesthetic treatments for a pleasing look.
- Encasement walls will help with river debris and ice loads.

The disadvantages of encased pile bent piers include the following:

- Encased pile bent pier heights are limited due to pile stability/flexibility issues. Calculations need to be made to ensure that the pile bent meets all of the design requirements. A rule of thumb is 20 ft from the top of the pier to the streambed (accounting for scour). Pile diameters can be increased to help with this issue but would still need to meet design requirements. The encasement wall should not be considered when designing for pile stability/flexibility.
- Encasement wall forms are not meant to need cofferdams and the like (but some protection may be needed). In some cases, it may be prudent to provide a foundation preparation pay item to allow for wall construction.

- Encased pile bent piers may not be adequate for longer spans, where the loads are greater.

The Wisconsin Department of Transportation (WisDOT) indicates that an advantage of encased pile bent piers is that the concrete encasement wall provides greater resistance to lateral forces than a pile bent (WisDOT 2023). Also, the hydraulic characteristics of this pier type are superior to those of pile bents, resulting in a smoother flow and reducing the susceptibility of the pier to scour at high water velocities. Another advantage is that floating debris and ice are less likely to accumulate against a pile-encased pier than between the piles of a pile bent. In the state of Wisconsin, pile sections used for encased pile bent piers are limited to 10 in., 12 in., or 14 in. steel HP piles, or 10¾ in., 12¾ in., or 14 in. diameter cast-in-place concrete piles with steel shells. The minimum center-to-center spacing is 3 ft. A minimum of five piles per pier must be used. The piles must be driven vertically. The total pier height must be less than 25 ft. The concrete wall must be a minimum of 2 ft 6 in. thick. The top 3 ft of the wall is made wider if a larger bearing area is required. The bottom of the wall must be placed 2 ft to 4 ft below stable streambed elevation, depending upon stream velocities and frost depth.

Liu et al. (2021b) conducted field monitoring on the fully encased pile bents of a bridge on IA 1 over Old Man's Creek during the sliding of the bridge superstructure. This project demonstrated, in part, the collective structural performance of steel piles and associated concrete encasement when subjected to the loads of a superstructure slide. Figure 2-4 shows the superstructure and substructure of the IA 1 bridge. The overall goal of this work was to identify and develop economic and durable design details to be used with the lateral slide concept, focusing on pier connection details. The focus was to capture the behavior and effects of the slide on key structural elements, including individual steel piles and the full pier wall assembly.

Figure 2-5 shows a bridge pier design drawing for the IA 1 bridge. The bridge pier consists of two wall piers founded on (14) HP16 x 101 driven piles. The bridge piles were placed with the weak axis parallel to the bridge longitudinal direction. All bridge piles are about 95 ft long and were placed with a spacing of 3.5 ft. The pier wall is 2.5 ft thick and 23 ft tall, including the pier cap.

During the lateral slide, higher strain magnitudes were observed at the pile locations immediately below the concrete encasement. Even so, the resulting forces were well below the maximum allowable forces. The residual axial and moment forces from the lateral superstructure slide were low in comparison to the capacity. An uplifting action was captured on one of two bridge piers. An approximate calculation indicated that the greatest forces realized in the longitudinal direction induced by the impulse-pushing load at the top of the pier were about 400 kips, with approximately 80 kips of residual force after the slide. Pier 1 had larger strain responses than Pier 2 in both the longitudinal and transverse directions of the bridge. This could be explained by multiple reasons, such as the different pier heights above grade, different friction coefficients, or uneven weight distribution. No noteworthy response from the substructure was observed during the slide-in. No visible signs of distress (e.g., cracking) were observed on the piers or at the bridge deck level. One of the conclusions of this study was that the substructure provided sufficient strength, stiffness, and resiliency to withstand the temporary and operational-induced forces accompanying the lateral slide-in method without negative or adverse effects.

(a) Superstructure of IA 1 bridge

(b) Substructure of IA 1 bridge with bridge orientation

Figure 2-4. IA 1 bridge piers

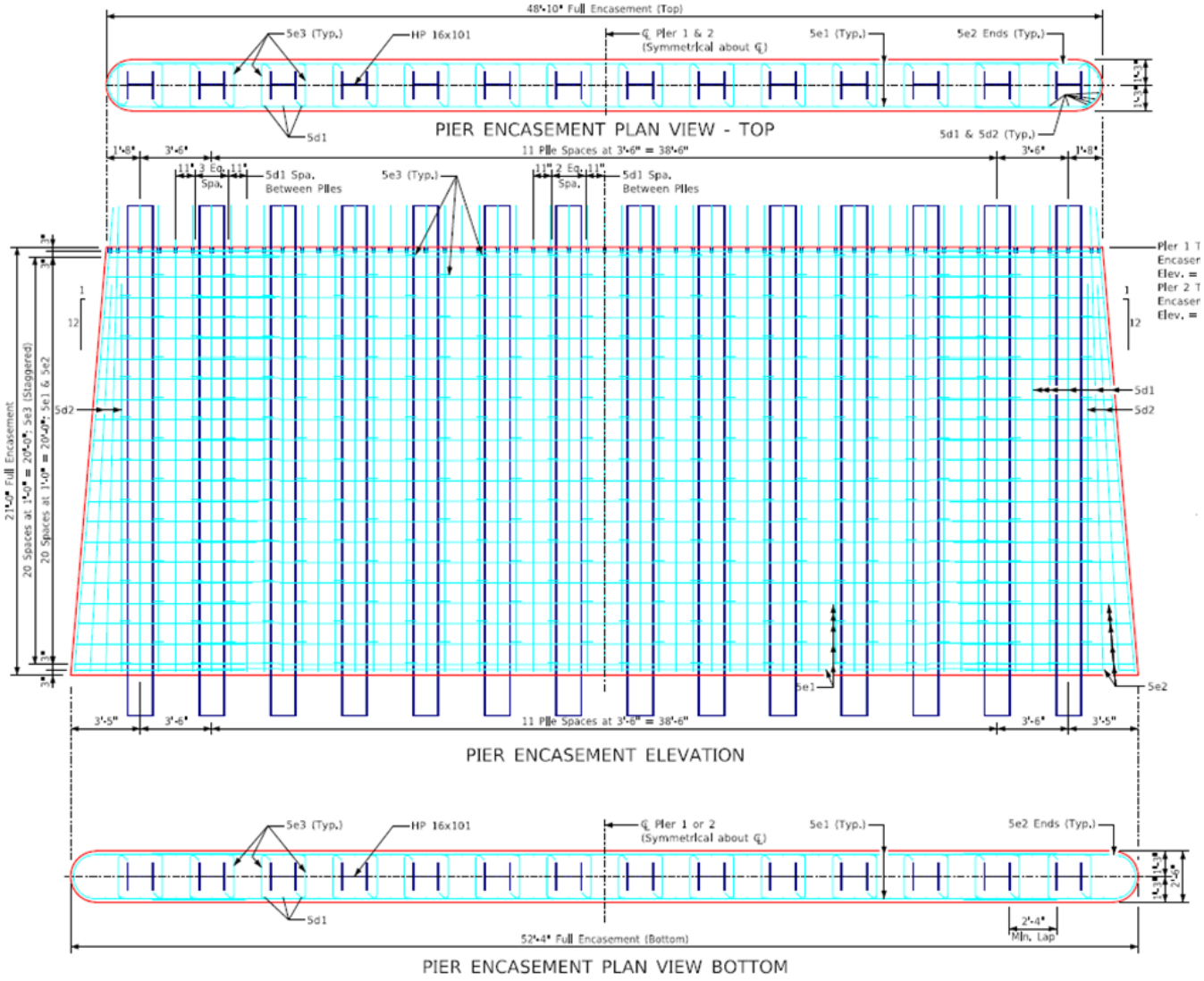

Figure 2-5. IA 1 bridge pier design drawing

3 LABORATORY INVESTIGATION OF FULLY ENCASED PILE BENTS

In previous research projects conducted at Iowa State University (Deng et al. 2018, Liu et al. 2021a), an assessment tool for singly encased piles was developed and validated through laboratory testing. The concrete encasement used in the tool's development is based on the P10L standard, which is the current Iowa design standard for pile bents with steel H-piles. The P10L standard specifies standard dimensions for specific pile sizes, which can be either square or round in cross-section. Accordingly, the capacity of piles in nonstandard encasement sizes or in fully encased pile bents is not directly calculated but rather inferred from the other calculations. The tool was developed through analysis and laboratory validation. In a similar way, analysis and laboratory validation can be completed to address pile capacities beyond those in standard encasements.

The present study expanded the scope of the previous research projects into the assessment and design of piles with fully encased piles. As part of this effort, an FE modeling approach was used to investigate inelastic buckling, elastic buckling, and plastic yielding in fully encased piles. Similar to the work in the previous research, the FE models were developed and validated against laboratory testing results. Further, numerous finite element models were created to ensure that multiple combinations of encasements and pile exposure conditions were considered. This analysis work is reported in Chapter 4.

In fully encased pile bents, the cross-sectional dimensions of the concrete encasement are greater than the P10L standard dimensions, and therefore the concrete contributes greater stiffness to the encased portion. Additionally, adjacent piles are positively connected through the encasement. The influence of additional encasement size and adjoining piles on the capacity of any single pile is unknown. Therefore, the laboratory testing in the present study was designed to enable direct comparison with the results of the previous study, where the P10L standard was used for the test specimens.

The specimen details from Liu et al. (2021a) are shown in Table 1.

Table 1. Specimen details from previous pile capacity investigation

Specimen	Section	Pile length (ft)	Encasement length (ft)	Experimental (kips)
1	HP10×42	16	N/A	612
2	HP10×42	16	10	715
3	HP10×42	30	20	563
4	HP10×42	38	30	606

Source: Liu et al. 2021a

In the present study, a test was completed that specifically investigated the system behavior of fully encased pile bents. This involved constructing a specimen similar to Specimen 3 from Liu et al. (2021a), which consisted of an HP10x42 pile with a total length of 30 ft and an encased length of 20 ft. However, instead of using the original P10L encasement, the pile was encased with two additional HP10x42 piles, which were arranged with a spacing and concrete cross-

section consistent with those of a fully encased pile bent, simulating system behavior. The load was applied at the pile bottom, allowing the research team to determine how loads are distributed between adjacent piles within the encasement.

An additional test for the present study investigated the behavior of an individual pile. Using the same specimen, the two additional piles were removed, leaving only the central pile. The central pile was then individually loaded in a manner similar to that of the first laboratory study. In this way, the capacity results could be directly compared to those of the previous specimen, and the influence of the encasement and additional piles could be determined.

3.1 Test I: Three-Pile Assembly

The test design, specimen construction, test setup, loading configuration, and instrumentation plan for the first test are presented and discussed in Sections 3.1.1, 3.1.2, 3.1.3, and 3.1.4, respectively. The test results are presented and discussed in Section 3.1.5.

3.1.1 Test Setup and Loading Configuration

To evaluate the behavior of the three-pile assembly, a controlled experiment was conducted. The three-pile assembly used in this study was constructed at full scale, representing potential in-field conditions. The vertical clearance of the laboratory and the load frames limited the ability to test the specimen vertically. Accordingly, a horizontal test setup and loading configuration were required to facilitate loading while remaining within the spatial constraints. This assembly is shown in Figure 3-1.

To accommodate the horizontal test setup and loading configuration, large concrete blocks were required to transfer the axial load to the floor. To increase frictional resistance at the floor interface, the blocks were post-tensioned utilizing the reaction floor, as the deadweight of the blocks alone lacked sufficient resistance. The post-tensioning process increased the frictional force between the blocks and the floor, preventing movement. Large blocks were placed at the pinned end and fixed end to provide resistance in two horizontal axes. The reaction blocks are labeled B1, B3, B5, and B6 in Figure 3-1.

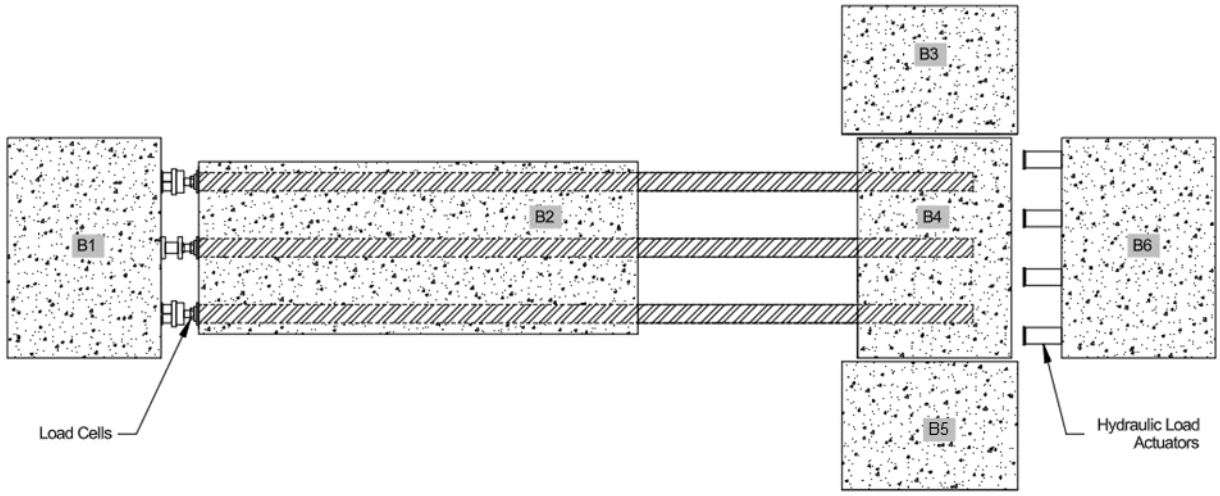

Figure 3-1. Three-pile assembly reaction blocks, load cells, and actuators

Obtaining accurate measurements of the load distribution among the three-pile assembly was critical. However, direct measurement at the fixed end was not feasible because the piles were embedded in concrete at that location. To address this, the test setup was designed so that the axial loads were applied from the fixed end, allowing load cells to be placed at the pinned end, where measurements could be taken more easily.

Figure 3-2 shows the pinned end of the test setup and block B1, which was used as the reaction block resisting the applied axial force. Three load cells were mounted horizontally on support block B1, each aligned with one of the test piles. The load cells were used to accurately measure the force in each pile during testing.

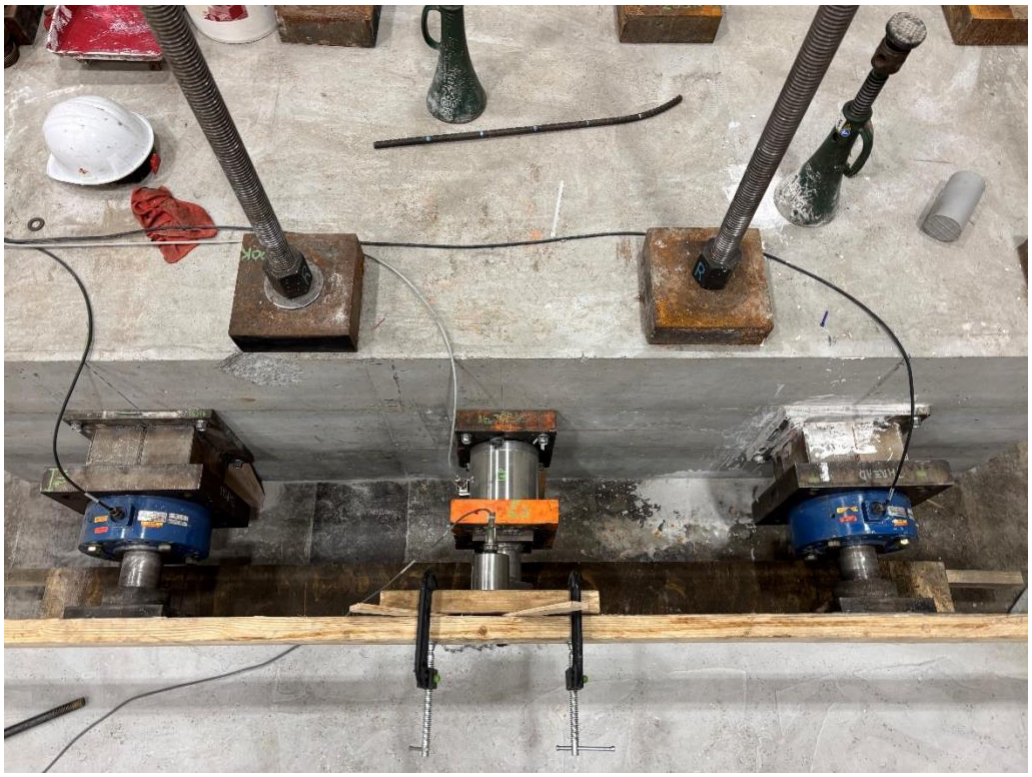

Figure 3-2. Pinned-end setup

Figure 3-3 depicts the fixed end of the test setup and block B6, which was used as the reaction block resisting the applied axial force. Four hydraulic actuators, each with a capacity of 200 kips, were mounted horizontally on block B6. These actuators were evenly spaced to ensure uniform application of axial force across the fixed-end condition.

Figure 3-3. Fixed-end setup

Based on prior research by Castilla et al. (1984), an embedment depth of 2 ft was considered to be sufficient to create a fixed-end condition. For this test, the piles extended 5 ft into the fixed-end concrete block, providing a more conservative embedment depth.

Two large rollers were placed between side blocks B3 and B5 and the central embedment block B4. These rollers allowed controlled movement in the axial direction. Additionally, a thin, greased Lauan sheet was placed beneath the embedment block to minimize friction between the block and the floor.

3.1.2 Test Design

The objective of this test was to evaluate the system behavior of the three-pile model, which was designed to represent a fully encased pile bent subjected to concentric axial loading, and to collect data for use in validating a finite element model. This setup simulates the load-bearing behavior of bridge substructures, where axial loads from the superstructure are transferred through the pile bents into the foundation. The test specimen consisted of three piles in a concrete encasement intended to provide stiffness and facilitate load distribution among the piles. To allow for future single-pile testing, axial loads were limited to service-level conditions, ensuring that the piles remained within the linear-elastic range. The test was primarily designed to evaluate how system-level loads are distributed among the three piles utilizing load, strain, and displacement data collected on the assembly.

Figure 3-4 shows the layout and boundary conditions of the three-pile assembly. The piles were labeled south pile (S1), middle pile (M2), or north pile (N3) to track responses throughout

testing. The central portion of the piles was fully encased in reinforced concrete. Outside the encasement region, the piles extended into an unencased region that simulated scour conditions. Boundary conditions were designed to simulate structural constraints; the top of the encasement was pinned to represent a connection to the bridge superstructure, while the base of the piles was fixed to represent an in-ground condition.

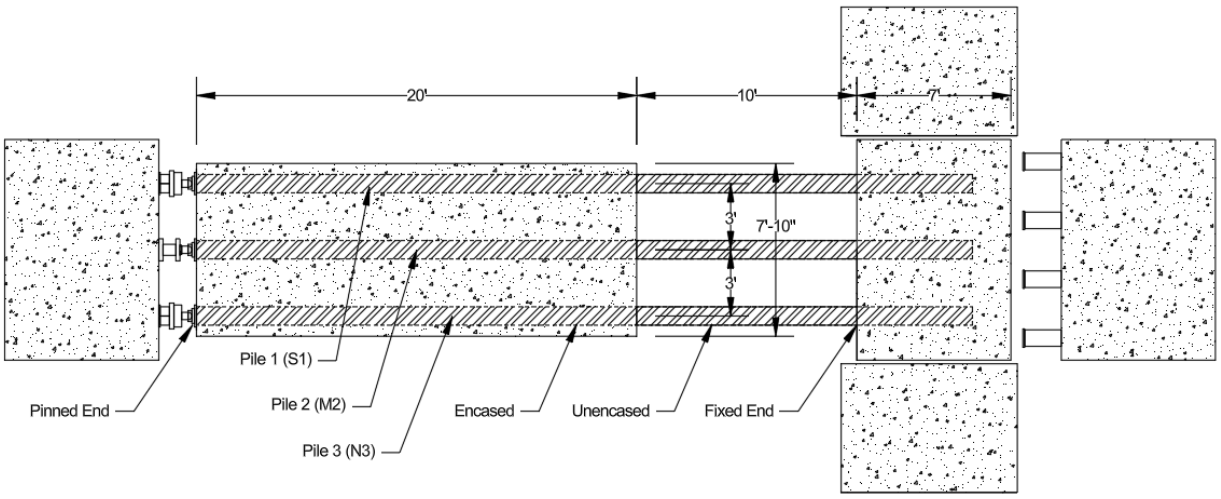

Figure 3-4. Layout and boundary conditions for the three-pile assembly

3.1.3 Assembly Construction

To begin the construction process of the pile encasement shown in Figure 3-5, three 30 ft HP10x42 steel H-piles were suspended and positioned on support blocks. This setup created the clearance for installing both the formwork and steel reinforcement. See Figure 3-6 and Figure 3-7. Once the piles were set, the formwork was assembled around them to shape the full concrete encasement and the fixed-end condition, replicating the structural constraints. Steel reinforcement was then installed within the formwork at specified locations determined per the American Association of State Highway and Transportation Officials (AASHTO) *LRFD Bridge Design Specifications* and the Iowa *Bridge Design Manual*. There were no additional mechanical connections made between the piles and the concrete encasement. With the formwork and reinforcement in place, concrete was cast in place, encasing the piles and completing the construction of the specimen. Figure 3-8 shows the three-pile specimen after construction.

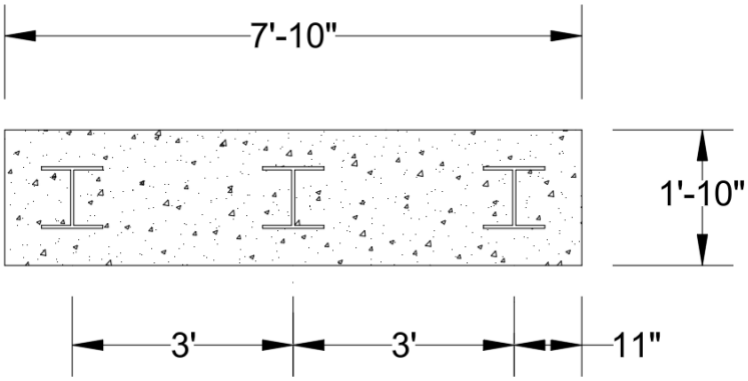

Figure 3-5. Cross-section at encased piles

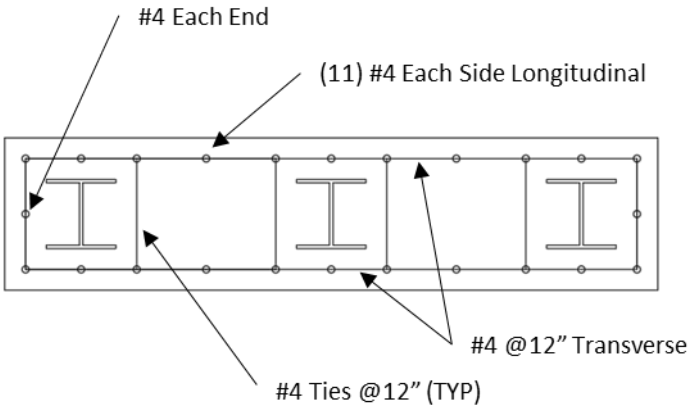

Figure 3-6. Pile encasement reinforcement

Figure 3-7. Pile encasement construction

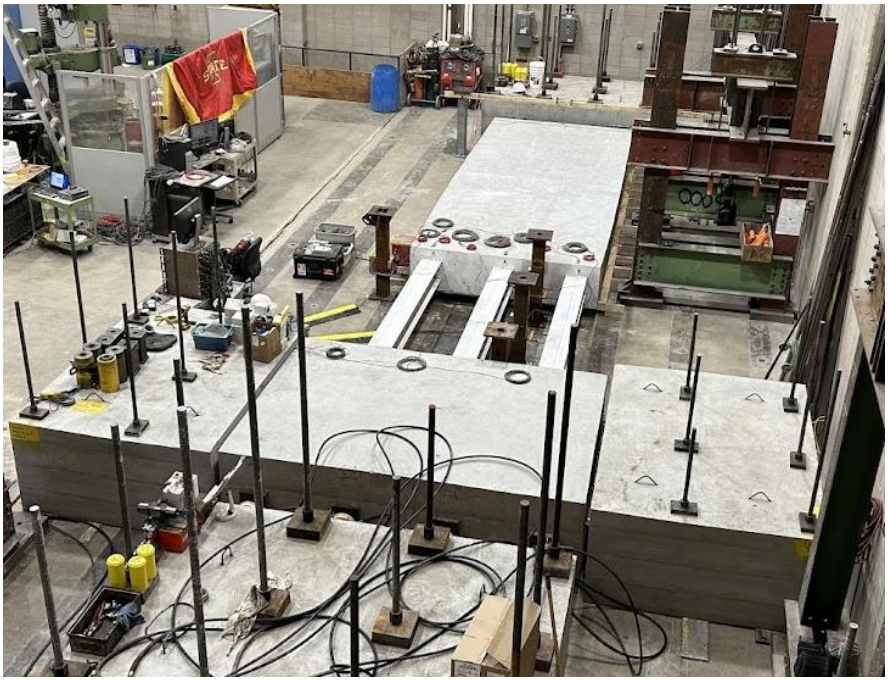

Figure 3-8. Completed three-pile assembly

3.1.4 Instrumentation Plan

Strain gages, displacement transducers, and load cells were placed along the specimen to observe the behavior of the specimen when loaded. The strain gages measured the strain of the unencased steel and concrete encasement when the axial load was applied, while each of the displacement transducers measured the amount of movement that occurred between a point of interest and a reference position. The hydraulic actuators applied the axial load, while the load cells measured the axial load at each of the three HP10x42 piles. All data collected by the devices were recorded and later analyzed.

To establish the locations of the strain gages and displacement transducers along the specimen, a number of cross-sections were created. Shown in Figure 3-9 are the five cross-sections viewed from the top of the specimen. From left to right, the cross-sections are Pin (P), Concrete (C), Middle (M), H (H), and Fix (F).

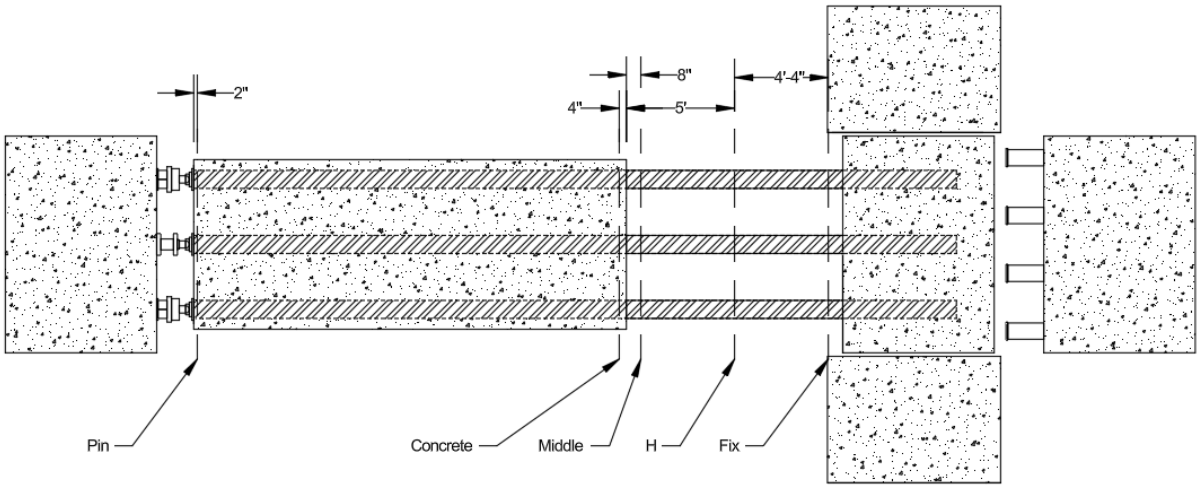

Figure 3-9. Three-pile assembly cross-section locations

Strain and displacement data were collected at several of the established cross-sections. Typical strain gage installation locations include the top flange, the middle of the web, and the bottom flange.

To organize the strain gage locations based on the cross-section, location, and direction, a naming system was created using a combination of letters. The letters for the cross-sections are P (Pin), C (Concrete), M (Middle), H (H), and F (Fix). The letters for the locations are T (Top), W (Web), and B (Bottom). Finally, if there was more than one gauge at a location, an additional letter was provided for the direction, N (North) or S (South). Additionally, the letter V indicates a displacement transducer located on the underside of a pile, while PD indicates a pile displacement transducer. The naming convention is summarized in Figure 3-10.

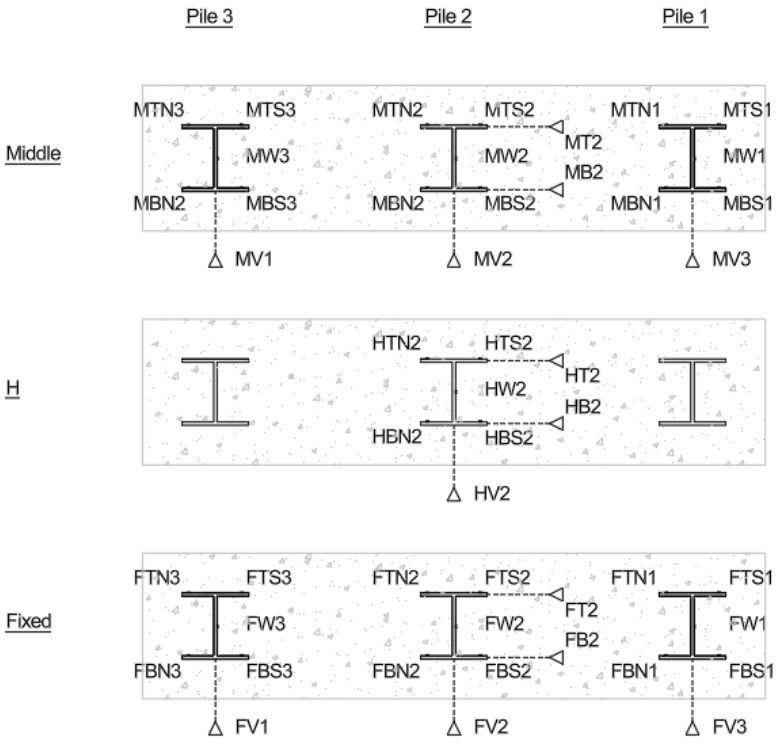

Figure 3-10. Strain and displacement gage locations (encased piles beyond)

On Piles 1 (S1) and 3 (N3), 10 strain gauges and two displacement transducers were placed. On Pile 2 (M2), 15 strain gauges and 9 displacement transducers were placed. The strain gauges were present at three cross-sections: Middle, H, and Fix. Displacement transducers measured vertical displacement at sections Middle and Fix for each pile and at section H for Pile 2. Horizontal displacement was measured at the top and bottom flanges of Pile 2. An additional displacement transducer was used to measure the pile shortening between the encasement and fixed-end concrete. Table 2 lists each strain gauge and displacement transducer and their locations.

Table 2. Gauge labels, type, and location

Label			Type	Location
PD1	PD2	PD3	Displacement	Bare Piles
MTN1	MTN2	MTN3	Strain	Middle
MTS1	MTS2	MTS3	Strain	Middle
MW1	MW2	MW3	Strain	Middle
MBN1	MBN2	MBN3	Strain	Middle
MBS1	MBS2	MBS3	Strain	Middle
-	MT2	-	Displacement	Middle
-	MB2	-	Displacement	Middle
MV1	MV2	MV3	Displacement	Middle
-	HTN2	-	Strain	H
-	HTS2	-	Strain	H
-	HW2	-	Strain	H
-	HBN2	-	Strain	H
-	HBS2	-	Strain	H
-	HT2	-	Displacement	H
-	HB2	-	Displacement	H
-	HV2	-	Displacement	H
FTN1	FTN2	FTN3	Strain	Fix
FTS1	FTS2	FTS3	Strain	Fix
FW1	FW2	FW3	Strain	Fix
FBN1	FBN2	FBN3	Strain	Fix
FBS1	FBS2	FBS3	Strain	Fix
-	FT2	-	Displacement	Fix
-	FB2	-	Displacement	Fix
FV1	FV2	FV3	Displacement	Fix

Figure 3-11 shows the placement of the displacement transducers, PD1, PD2, and PD3, along the length of the bare pile, and the top, bottom, and vertical transducers, located at the Middle, H, and Fix sections, fastened to the steel pedestals along the length of the unencased portion of the specimen.

Figure 3-11. Displacement transducers

In addition, the surface of the three HP10x42 steel piles was prepared for testing. A thin lime-based coating was applied to visually depict strain and deformation during loading; the coating cracks or flakes in areas of high stress or deformation. Figure 3-12 shows the lime-washed surfaces.

Figure 3-12. Lime-washed surfaces

3.1.5 Test Results

Initial Tests

The testing process began with the application of a low axial load to verify that all gauges and the data acquisition system were responsive and functioning correctly. The assembly was loaded slowly and then returned to its unloaded state. This process was repeated twice to gather sufficient data. Visual inspection of the unencased steel piles showed no signs of high stresses; the lime wash coating remained intact. Visual inspection of the concrete encasement and fixed-end block showed no cracking. This was expected, as the test was preliminary and not intended to push the specimen to the point of failure.

During the initial loading, the percentage of total load into the system and individual piles was measured. These data are plotted in Figure 3-13. It was expected that the load into the middle pile (M2) would be slightly higher than the load into the two outer piles (S1 and N3) and that the load into the outer piles would be nearly the same. The initial test results showed a greater deviation in the load between the outer piles than anticipated.

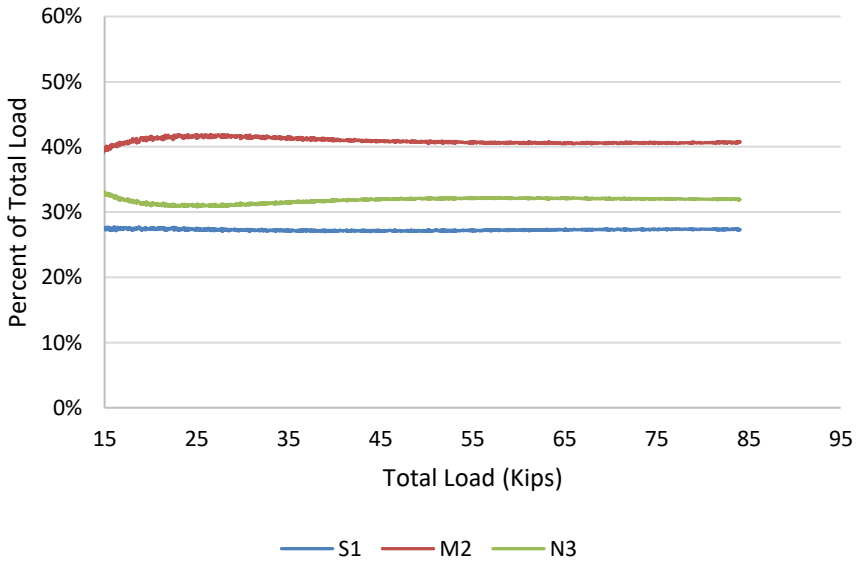

Figure 3-13. Percent of total load in each pile as total load increased – initial test

Even load distribution is important to prevent premature, localized failures within the specimen. It ensures that no single area is overstressed and allows for a more accurate assessment of the specimen's behavior under load. In theory, an even load distribution would imply that the two outside piles, while expected to experience loads slightly lower in magnitude than the load on the middle pile, should experience loads similar to each other. To correct any inconsistencies in the bearing at the load cells and to provide a more even load distribution between the two outside piles, Hydro-Stone was added at the interface of the load cell plates and the reaction block at

cells S1 and N3. The initial test was completed again, with the results indicating the loads in the outer piles were very close, as shown in Figure 3-14.

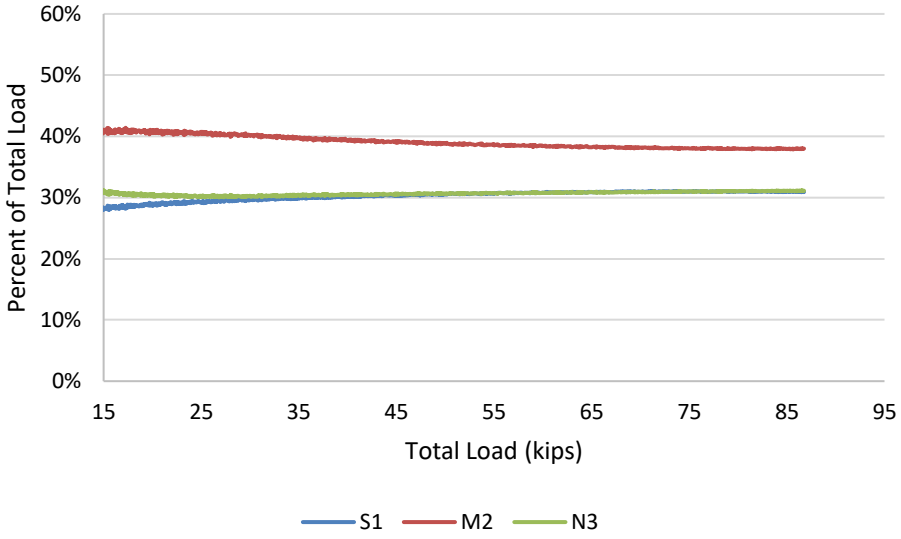

Figure 3-14. Percent of total load in each pile as total load increased – initial test 2

All gauges used during the initial test were confirmed to be responsive and functioning. Strain gauges on the piles at the Middle, H, and Fix sections provided consistent readings with no signal loss. Additionally, the recorded data showed a strong linear correlation between total load and measured microstrain, indicating that the specimen remained in the elastic range.

Final Tests

Once the initial tests were completed, the three-pile assembly was subjected to the maximum load that could be applied with the four load actuators of nearly 800 kips. The load distribution between piles was calculated, and the strain and displacement data were analyzed.

A visual inspection of the exposed steel piles revealed no indications of stress, as the lime wash coating remained intact. Similarly, the concrete encasement and end block showed no visible cracking. As with the preliminary loading, the specimen showed no visible distress in the steel piles and concrete encasement, which suggests good structural performance under the applied axial load.

As the load increased, the load distribution varied slightly, but overall it remained more consistent throughout the testing process. Figure 3-15 shows the loads in each pile, S1, M2, and N3, as the total load increased. The maximum loads measured were 264.8 kips in the south pile (S1), 275.1 kips in the middle pile (M2), and 248.4 kips in the north pile (N3). The maximum total load was 788.1 kips. To further illustrate the loading, Figure 3-16 shows the percent of total load for each cell as the total load increased. The percent of the total load measured in each pile

was 34%, 35%, and 32% for S1, M2, and N3, respectively. The load data suggest that the load was distributed evenly.

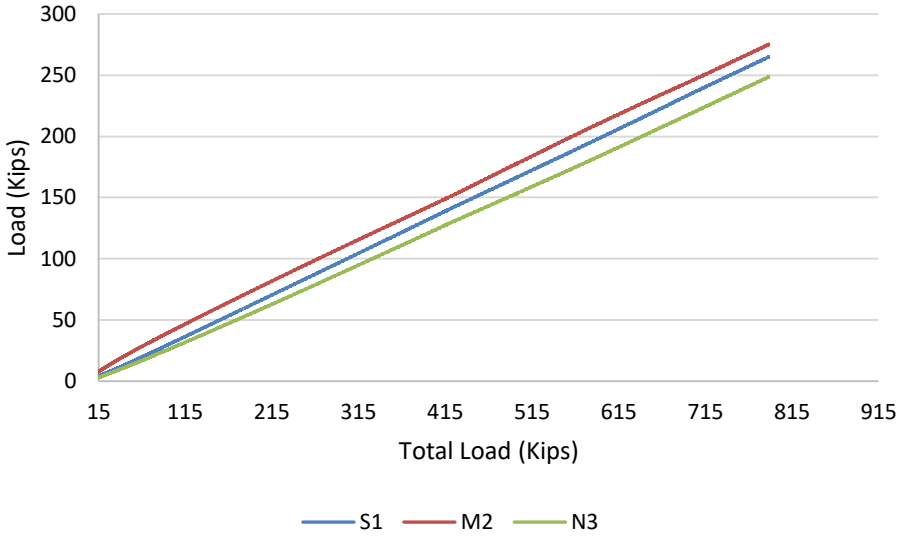

Figure 3-15. Load in each pile as total load increased – final test

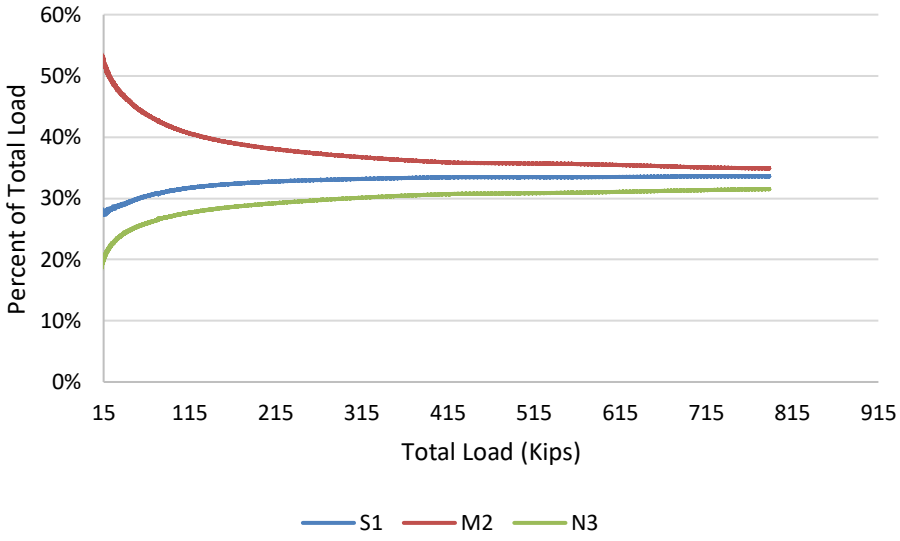

Figure 3-16. Percent of total load in each pile as total load increased – final test

Using the data collected from the load cells and strain gauges, stress versus strain data were plotted to evaluate the general pile behavior and to ensure that the piles remained in the linear elastic region of the stress-strain curve. The stress data were calculated by dividing the load data by the cross-sectional area of the member, which for a HP10x42 steel member is 12.4 in^2. The maximum calculated stresses in the south (S1), middle (M2), and north (N3) piles were 21.3 ksi, 22.2 ksi, and 20.0 ksi, respectively. Figure 3-17, Figure 3-18, and Figure 3-19 illustrate the stress

versus compression strain data for each of the piles at each of the instrumented cross-sections for the full load range (0 to 788 kips). Figure 3-20 illustrates the strain range at each instrumented cross-section at the peak stress.

Within this load range, the piles exhibit a clear linear elastic relationship, as shown by the constant slope, which represents the elastic modulus of the steel. There was no noticeable deviation from linearity, which indicates that the specimen remained within its elastic limit.

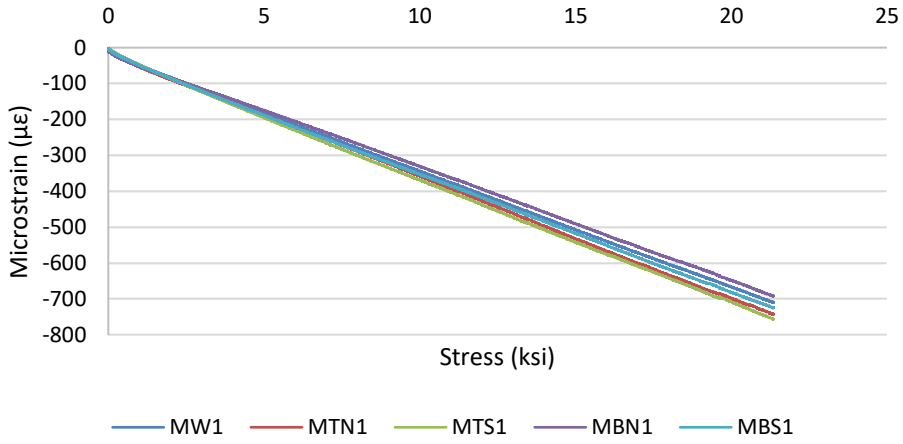

(a) Middle Section Pile 1

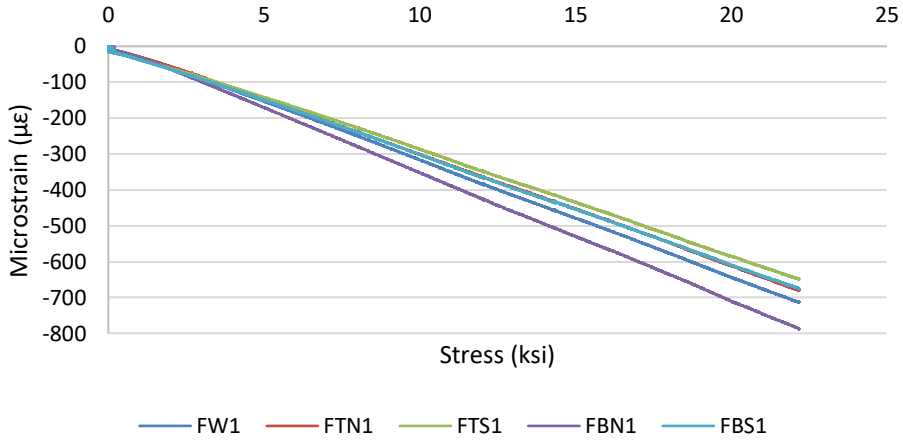

(b) Fixed Section Pile 1

Figure 3-17. Stress versus strain in unencased section of Pile 1 (N1)

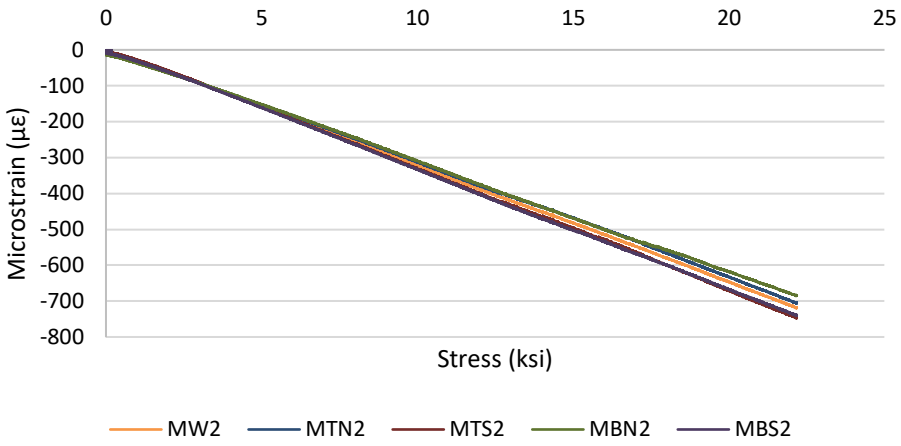

(a) Middle Section Pile 2

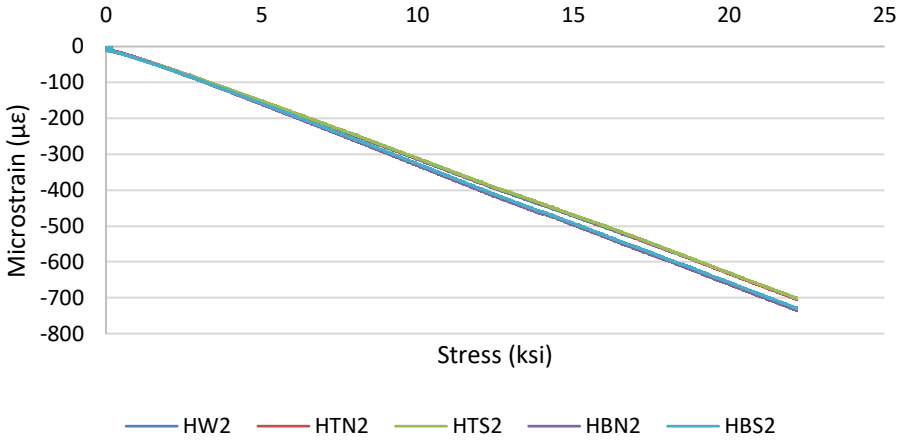

(b) H Section Pile 2

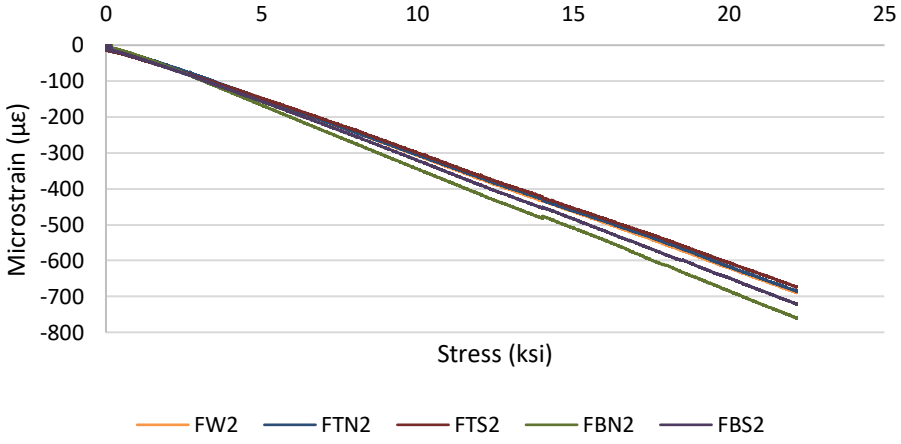

(c) Fixed Section Pile 2

Figure 3-18. Stress versus strain in unencased section of Pile 2 (N2)

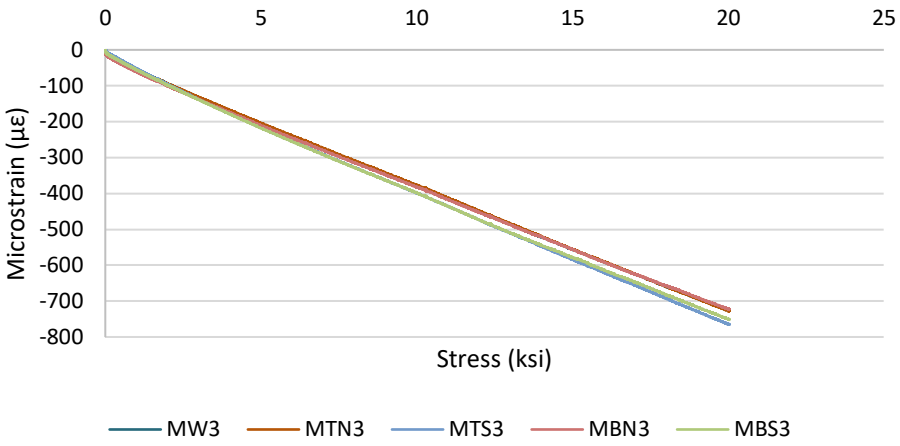

(a) Middle Section Pile 3

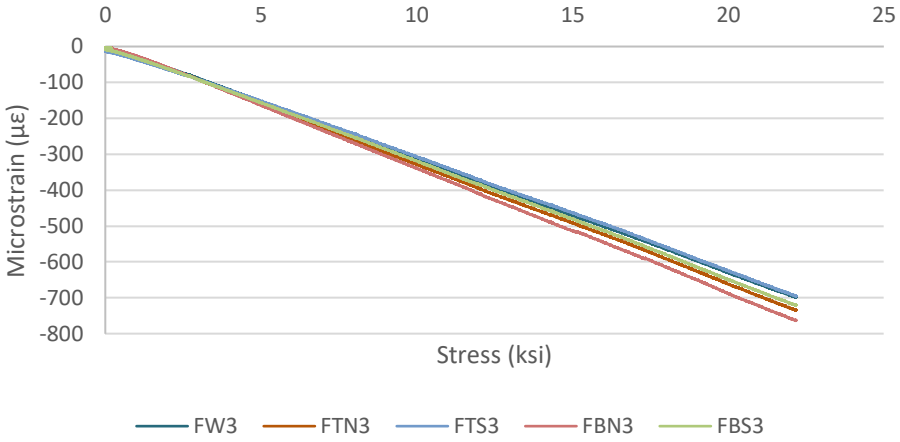

(b) Fixed Section Pile 3

Figure 3-19. Stress versus strain in unencased section of Pile 3 (N3)

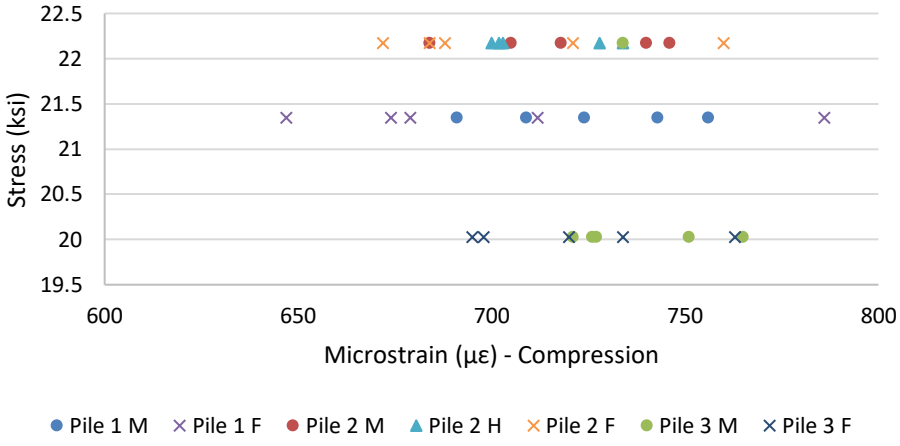

Figure 3-20. Three-pile assembly maximum stress and strain for each pile

Figure 3-21 presents the pile shortening of the unencased section of each pile during the full load range. The maximum displacements measured on Piles 1 (S1), 2 (M2), and 3 (N3) were 0.094 in., 0.095 in., and 0.099 in., respectively. Backcalculating the strains for the 120 in. length of the unencased section of each pile results in 783, 792, and 825 microstrain for Piles 1, 2, and 3, respectively. These values are slightly higher than the values shown in Figure 3-20, though within a reasonable range of acceptance. The remaining horizontal and vertical displacement gauges registered values no greater than 0.015 in., indicating that the piles did not effectively move in the horizontal or vertical direction.

It is noteworthy that the total load applied to each pile during this test exceeded the factored Structural Resistance Level 1 (SRL-1) design load of 107 kips by more than double.

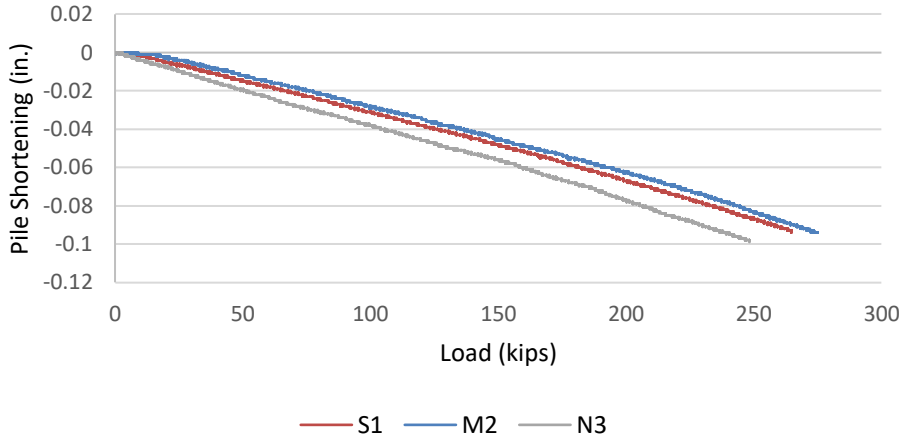

Figure 3-21. Pile shortening at unencased section during loading

3.2 Test II: Single-Pile Assembly

The test design, specimen construction, test setup and load configuration, and instrumentation plan for the second test are presented and discussed in Sections 3.2.1, 3.2.2, 3.2.3, and 3.2.4, respectively. The test results are presented and discussed in Section 3.2.5.

3.2.1 Test Design

The objective of this test was to evaluate the behavior of the three-pile assembly when only a single pile was subjected to loading. Structural members subjected to high axial loading can fail in several ways: yielding, elastic buckling, and inelastic buckling. The three failure methods are complex failure mechanisms that can occur independently or in combination. Yielding, which occurs when the applied axial load exceeds the material's yield strength, causing the structure to plastically deform, may occur before, during, or after buckling. Elastic buckling occurs when a structure under a high axial load undergoes reversible deformation, while inelastic buckling occurs when a structure undergoes irreversible deformation after the applied axial load has exceeded its proportional limit. In this test, the behavior of a single pile subjected to a high axial

load was assessed for the three failure methods utilizing load, strain, and displacement data along the length of the specimen.

Figure 3-22 shows the layout and boundary conditions of the single-pile specimen, which was modified from the original three-pile specimen. While all three piles remained encased in concrete, the unencased portion of the two outer piles, designated S1 and N3, were removed. Only the central pile, designated M2, remained unaltered for testing. The boundary conditions matched those of the three-pile test; the top of the encasement was pinned, representing a connection to the bridge superstructure, while the base of the piles was fixed to represent an in-ground condition.

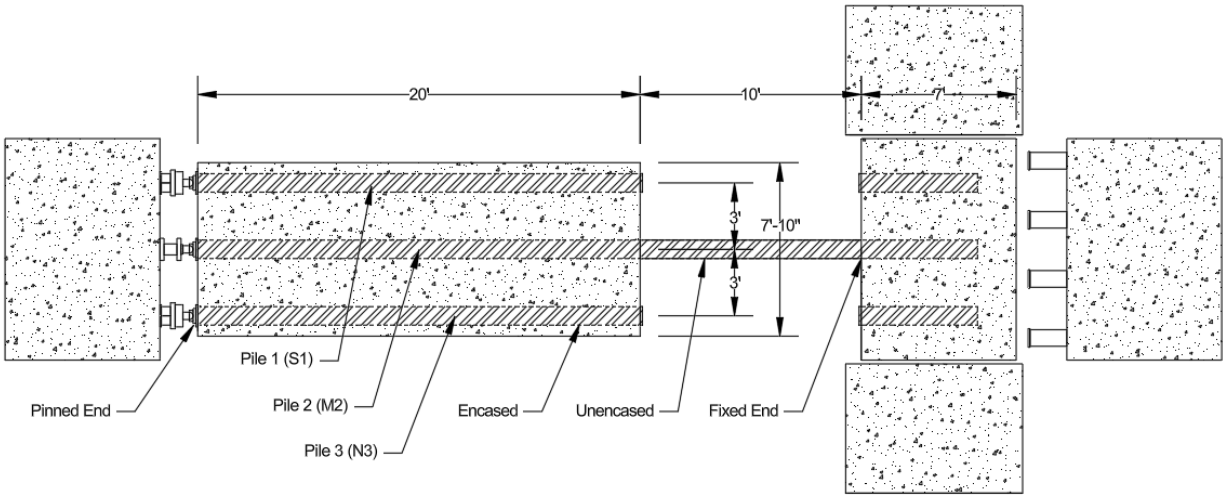

Figure 3-22. Layout and boundary conditions for the single-pile assembly

3.2.2 Assembly Construction

The single-pile specimen was constructed in the Structural Laboratory at Iowa State University as part of a controlled experimental setup. To eliminate the need for constructing a new specimen, the three-pile specimen from the previous test was modified for use in a single-pile test. The modification process involved removing the unencased portion of the outer piles, designated S1 and N3, leaving only the encased portion intact. The center pile, designated M2, remained unaltered and was subjected to axial load. This modification forced the center pile to carry all of the load, allowing evaluation of single-pile behavior.

To remove the unencased portion of the outer piles, the steel was cut using an oxyacetylene torch. The high-temperature flame produced by the torch ejects small, heated metal particles into the surroundings, commonly referred to as swarf. To control the swarf and protect nearby equipment, fire protection measures were implemented. The strain gauges and displacement transducers were protected by fire blankets, while the data logger was protected by a series of fire-resistant barriers. Figure 3-23 shows the single-pile specimen after the modification process.

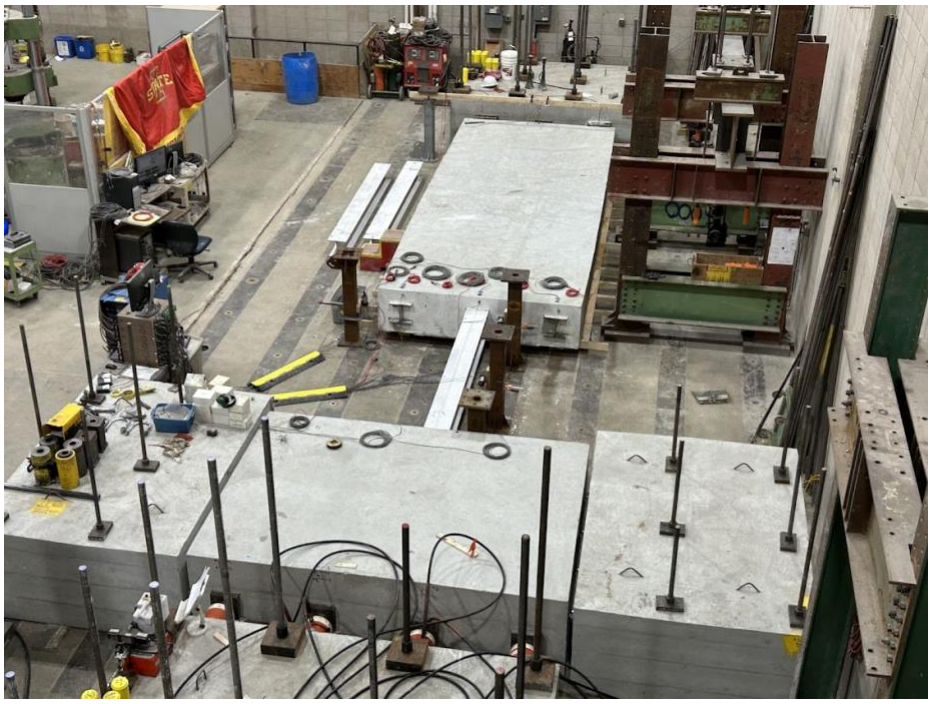

Figure 3-23. Single-pile specimen

3.2.3 Test Setup and Loading Configuration

To evaluate the behavior of the single-pile assembly, a controlled experiment was conducted. Similar to the previous study, the single-pile assembly was constructed at full scale, representing real-world conditions. The assembly, however, could not be tested vertically due to the vertical limitations of the laboratory. Instead, a horizontal test setup and loading configuration were implemented to facilitate loading while remaining within the limits of the laboratory.

Utilizing the same test setup and loading configuration as the previous study, large concrete blocks were positioned to transfer the axial load to the floor. To increase frictional resistance at the floor interface, the blocks were post-tensioned utilizing the reaction floor, as the blocks alone lacked sufficient frictional resistance. The post-tensioning process increased the frictional force between the blocks and the floor, preventing movement. Large blocks were placed at the pinned end and fixed end of the specimen to provide resistance in two horizontal axes. Figure 3-24 shows the numbers assigned to the blocks used to provide resistance in the single-pile test.

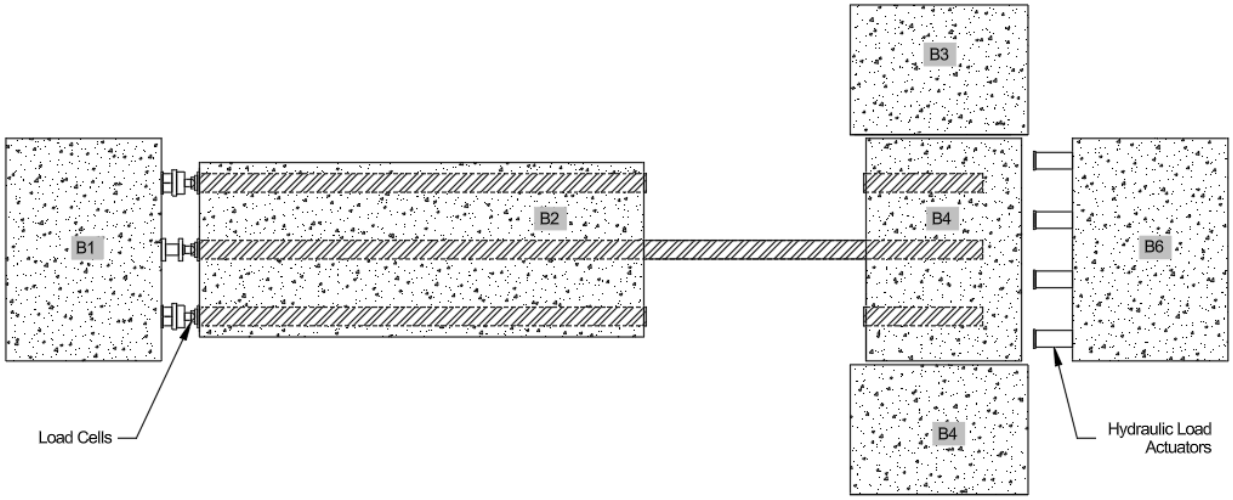

Figure 3-24. Single-pile assembly reaction blocks, load cells, and actuators

3.2.4 Instrumentation Plan

Strain gages, displacement transducers, and load cells had been placed along the three piles as part of the first test to observe the behavior of the assembly when loaded. The strain gages measured the strain of the unencased steel piles when the axial load was applied, while each of the displacement transducers measured the amount of movement that occurred between a point of interest and a reference position. The hydraulic actuators applied the axial load, while the load cells measured the axial load at each of the three HP10x42 piles. The strain gauges and displacement transducers along the unencased portion of the outer piles were removed for this test, and those on the center pile remained fixed and fully operational. All data collected by the remaining gauges and transducers were recorded and later analyzed.

The cross-sections used in the first test to establish the locations of the strain gages and displacement transducers were maintained along the length of the center pile, and the same measuring devices from the previous test were utilized. As shown in Figure 3-25, the five cross-sections viewed from the top of the specimen are, from left to right, Pin (P), Concrete (C), Middle (M), H (H), and Fix (F).

Figure 3-26 depicts the cross-sections designated for the single-pile test from Liu et al. (2021a) to serve as a point of comparison to the three-pile assembly used in the present study.

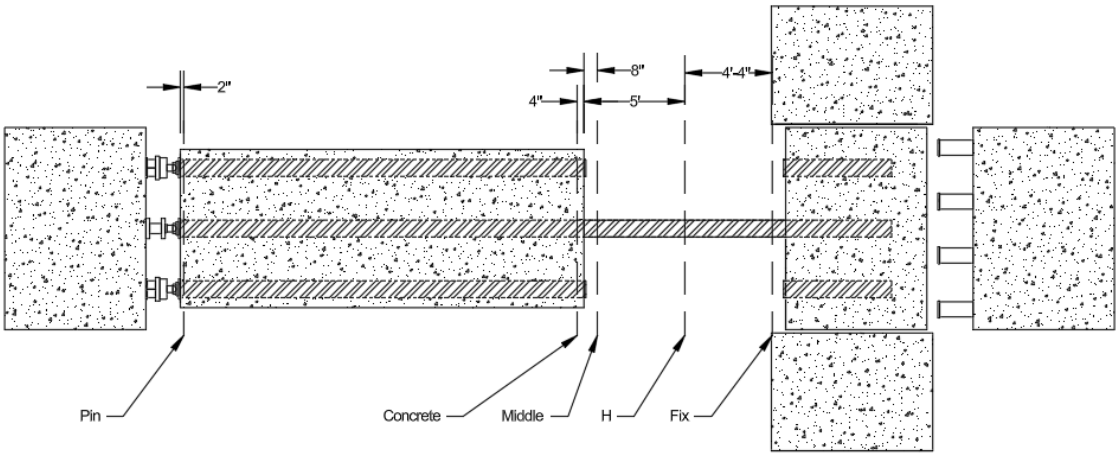

Figure 3-25. Single-pile assembly cross-section locations

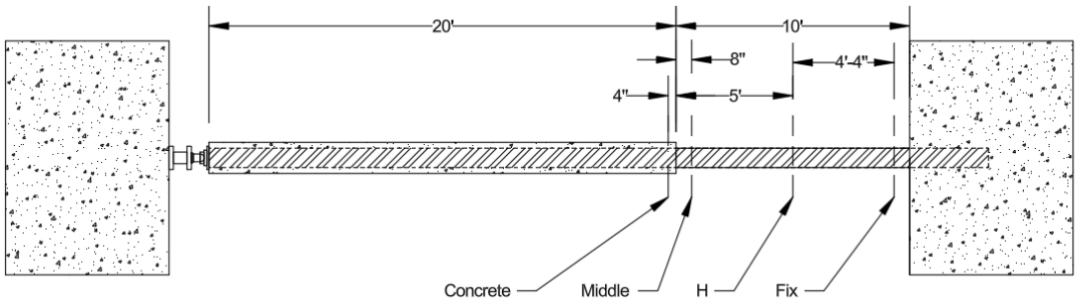

Liu et al. 2021a

Figure 3-26. Single-pile assembly – unencased

Strain and displacement data were collected at the established cross-sections. Strain gage and displacement transducer locations were organized using a consistent naming system in which letters were used to designate cross-sections (M [Middle], H [H], and F [Fix]) and locations (T [Top], W [Web], and B [Bottom]), with an additional directional letter, N (North) or S (South), assigned if multiple gages were present at a location. Figure 3-27 details the placement of strain gages and displacement transducers along the center pile. Figure 3-28 shows the gauge labeling used in Liu et al. (2021a) so that the data can be directly compared.

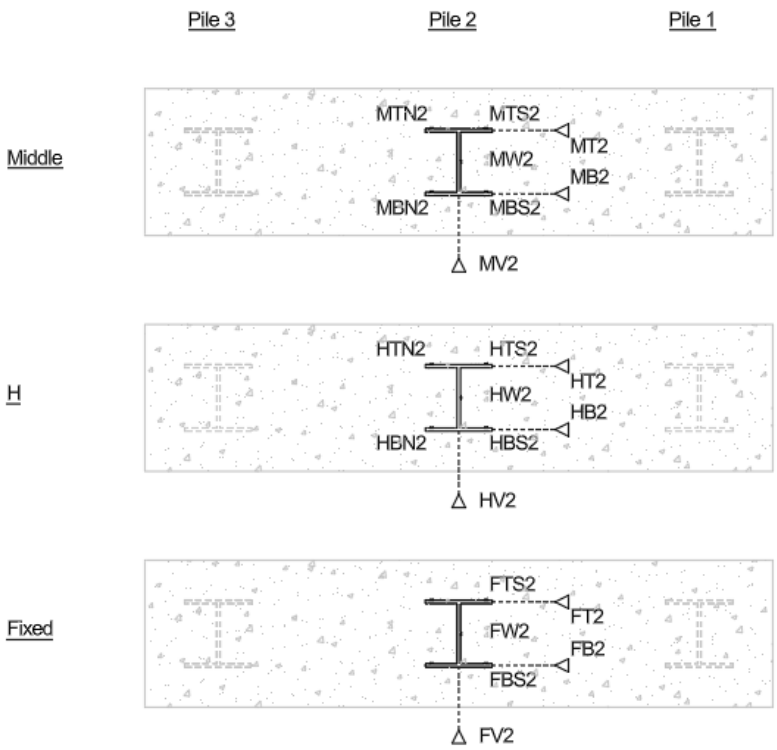

Figure 3-27. Strain and displacement gage locations (encased piles beyond)

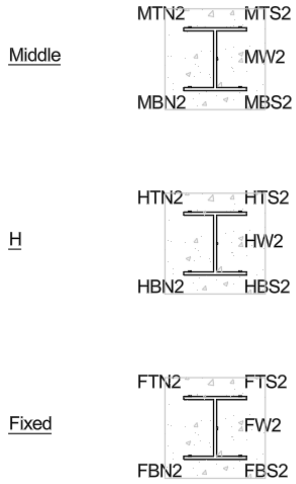

Liu et al. 2021a

Figure 3-28. Strain and displacement gage locations of P10L assembly

3.2.5 Test Results

The axial load was steadily increased until the maximum load was achieved, and the test then continued until the point of extensive deformation of the pile. Assuming an elastic modulus of 29,000 ksi and 50 ksi steel, the pile theoretically could be expected to begin yielding at 1,700

microstrain. Another way of looking at this is that the maximum load before yielding is 620 kips for a 50 ksi steel pile with a cross-sectional area of 12.4 in^2, assuming that another failure mechanism does not control.

Section E7 of the AISC specification for structural steel buildings (AISC 2012) prescribes the calculations for obtaining the nominal compressive strength, P_n, for slender element compression members. The flanges of an HP10x42 pile are considered slender based on the width-to-thickness ratio, b/t_f. Using these calculations, the strength of the pile can be calculated and compared to the laboratory results. The calculations are presented in Table 3 and Table 4.

For members with slender elements, the nominal compressive strength, P_n, is the lowest value based on the applicable limit states of flexural buckling, torsional buckling, and flexural-torsional buckling. Table 3 presents the calculations for this case.

Table 3. Nominal compressive strength of H-Pile with slender elements per AISC

The nominal compressive strength is:	$P_n = F_{cr}A_g$
The critical stress is:	$F_{cr} = Q\left[0.685^{\frac{QF_y}{F_e}}\right]F_y$
Because:	$\frac{KL}{r} \leq 4.71\sqrt{\frac{E}{QF_y}}$
The net reduction factor, Q, is calculated as:	$Q = Q_s Q_a$
With:	$Q_s = 1.0$
Because:	$\frac{b}{t} \leq 0.56\sqrt{\frac{E}{F_y}}$
Because the effective area and the gross cross-sectional area of the pile are equal:	$Q_a = 1.0$
The elastic stress is:	$F_e = \frac{\pi^2 E}{\left(\frac{KL}{r}\right)^2}$

For a 10 ft unencased HP10x42 with a fixed-end condition, the calculated nominal compressive strength is 593 kip, as shown by the calculations in Table 4.

Table 4. Calculated nominal compressive strength of HP10x42

Variables	Calculations
$E = 29{,}000\ ksi$	$\frac{KL}{r_y} = 24.9$
$F_y = 50\ ksi$	$\frac{b}{t} = 12.0$
$b = 5.05\ in$	$0.56\sqrt{\frac{E}{F_y}} = 42.6$
$t = 0.415\ in$	$Q = 1.0$
$r = 2.41\ in$	$F_{cr} = 47.8\ ksi$
$K = 0.5\ (Assuming\ Fixed - Fixed)$	$A_g = 12.4\ in^2$
$L = 120\ in$	$P_n = 593\ kip$

The single-pile assembly was axially loaded until it was unable to accept more load. The maximum load applied to the single-pile assembly was 668 kips. Prior to the maximum load being reached, the strain values for most gauges began to deviate from the linear load-to-strain relationship at approximately 620 kips, or near the theoretical yield point. This relationship can be seen in Figure 3-29, Figure 3-31, and Figure 3-33. Comparisons of the strain-to-load data collected in Liu et al. (2021a) for the P10L single pile to the data collected in the present study for the encased single-pile assembly are made in Figure 3-30, Figure 3-32, and Figure 3-34 at each of the three instrumented cross-sections. It is evident from these plots that the ultimate capacity of the encased pile is approximately 18% greater than that of the P10L assembly.

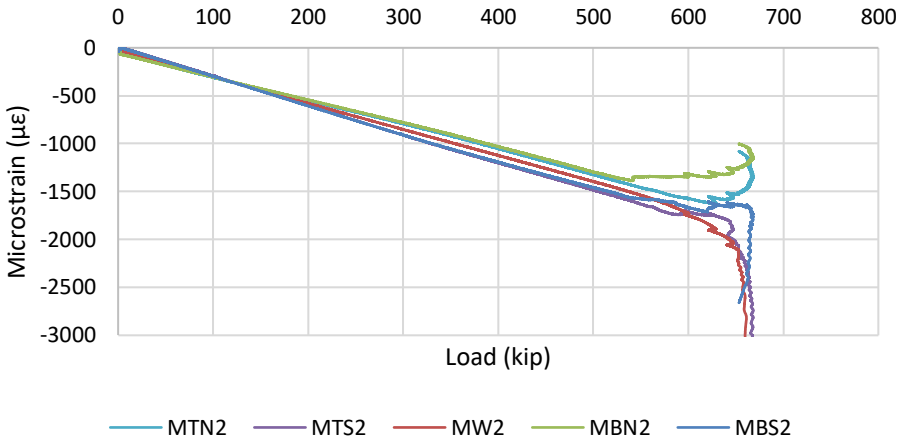

Figure 3-29. Strain versus load at section Middle

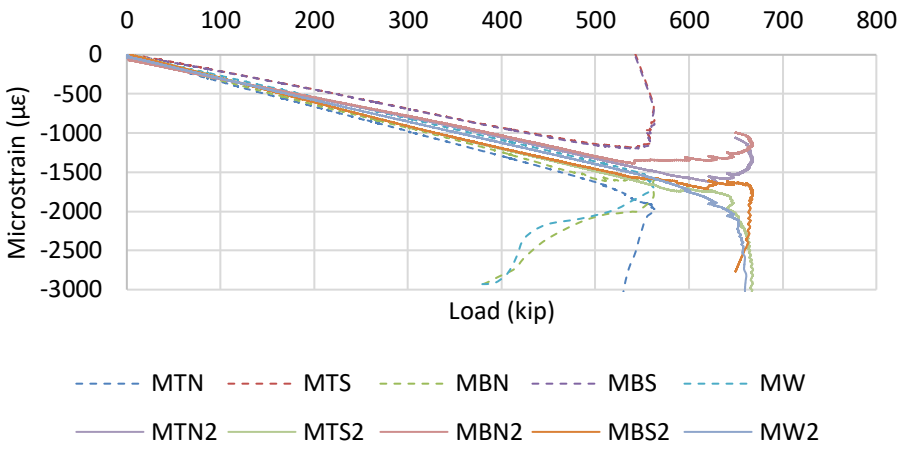

Figure 3-30. Comparison of strain versus load for unencased and encased pile assemblies at section Middle

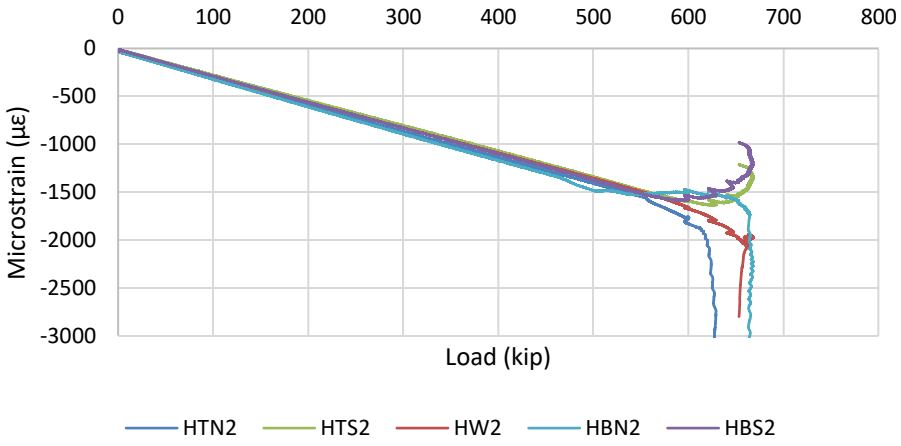

Figure 3-31. Strain versus load at section H

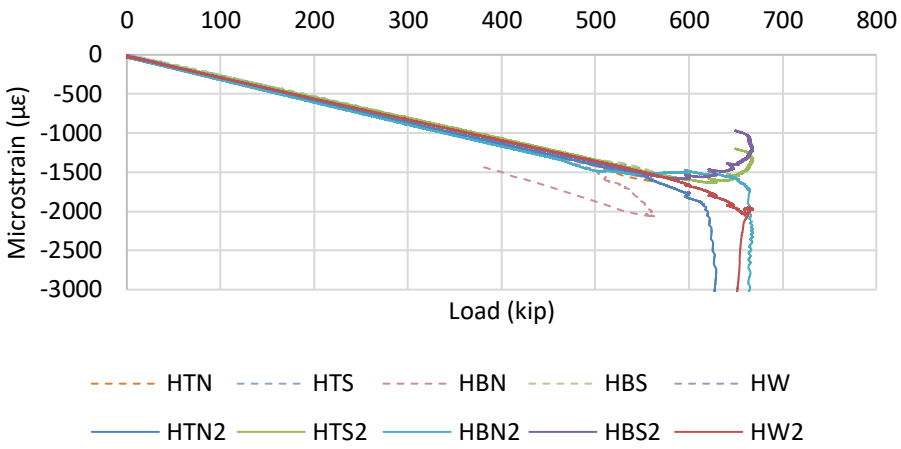

Figure 3-32. Comparison of strain versus load for unencased and encased pile assemblies at section H

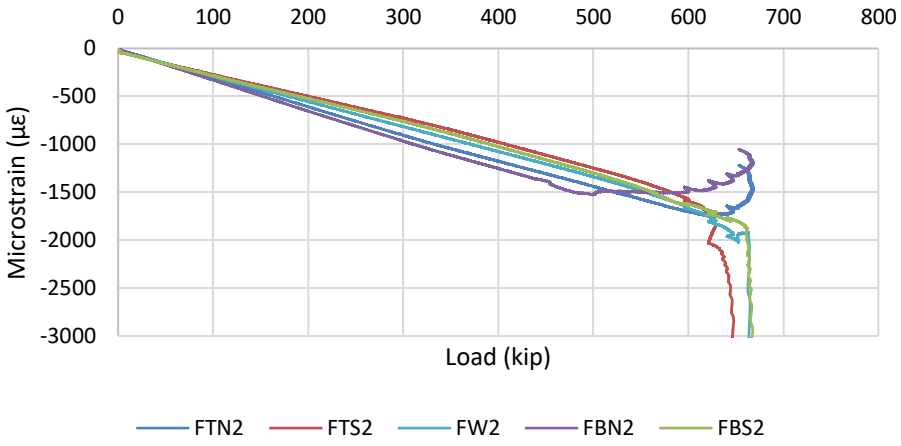

Figure 3-33. Load versus strain at section Fix

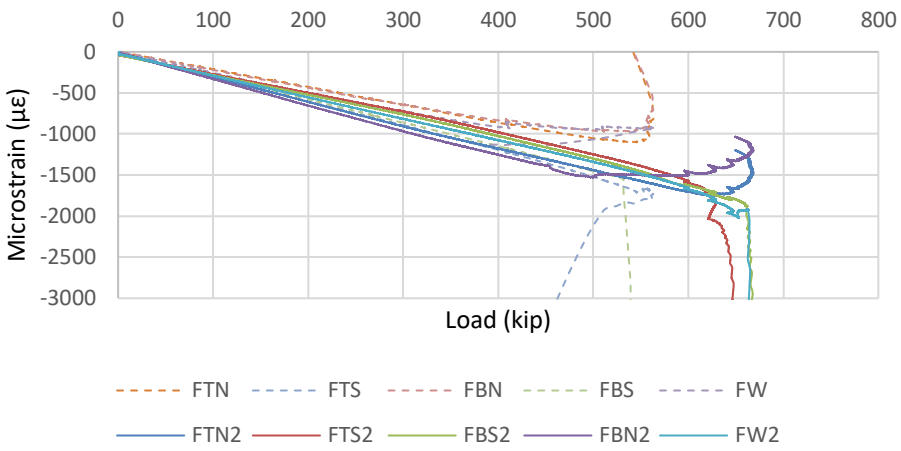

Figure 3-34. Comparison of strain versus load for unencased and encased pile assemblies at section Fix

Horizontal displacement of the pile flanges was measured during the loading at sections Middle, H, and Fix. The displacement values relative to the load in the pile are plotted for each section in Figure 3-35, Figure 3-36, and Figure 3-37, respectively. Figure 3-38 provides a comparison of the displacement values at each of the cross-sections. Much like the strain data, notable horizontal displacement does not begin until the load exceeds 600 kip or greater, and the unencased portion of the pile begins to locally and globally buckle.

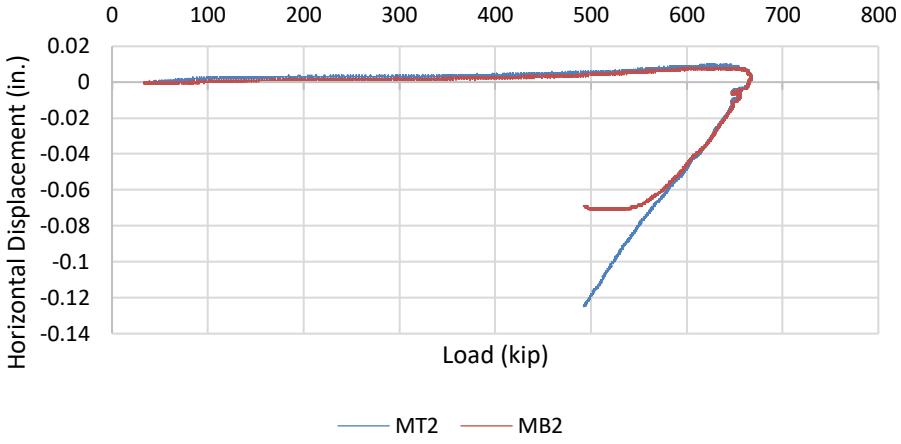

Figure 3-35. Horizontal flange displacement at section Middle

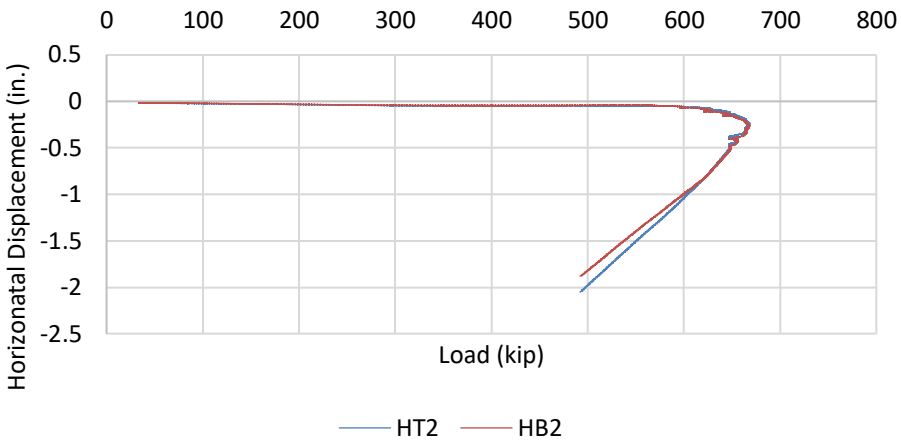

Figure 3-36. Horizontal flange displacement at section H

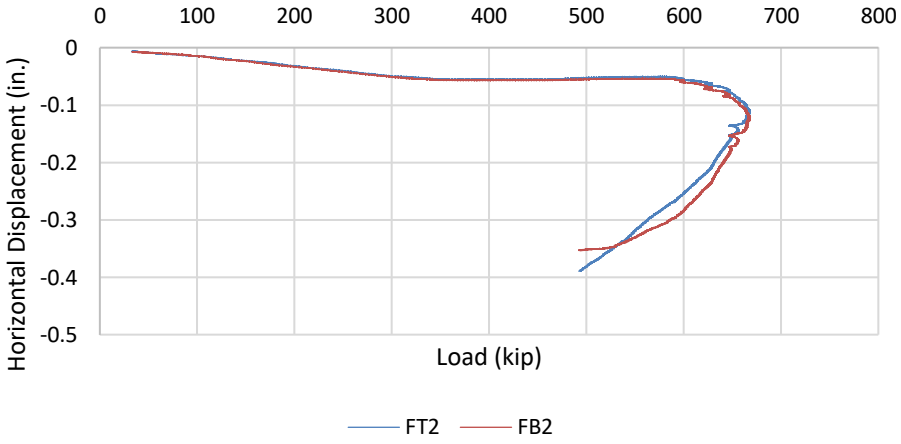

Figure 3-37. Horizontal flange displacement at section Fix

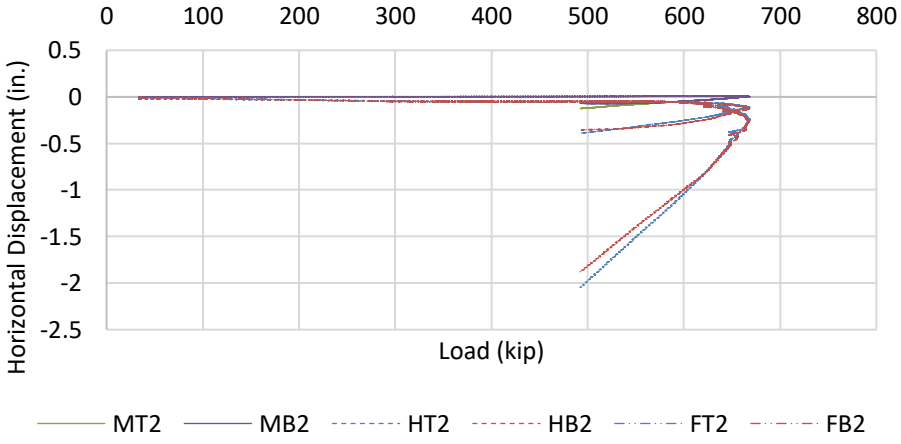

Figure 3-38. Comparison of horizontal flange displacement at sections Middle, H, and Fix

Prior to achieving the maximum load, visual inspection of the unencased portion confirmed signs of yielding as the lime wash developed transverse cracks on the flanges, as shown in Figure 3-39 and Figure 3-40.

Figure 3-39. Transverse cracks in the lime wash on bottom flange – 1

Figure 3-40. Transverse cracks in the lime wash on bottom flange – 2

After yielding became apparent, the test continued with more load put into the pile. At this point, the pile began to experience local flange buckling at the ends and middle of the unencased portion (sections Middle, H, and Fix). Simultaneously, the pile experienced global buckling as the middle of the unencased portion began to translate horizontally. The final state of the pile upon completion of the test is shown in Figure 3-41. Side views of the web and flanges are provided in Figure 3-42.

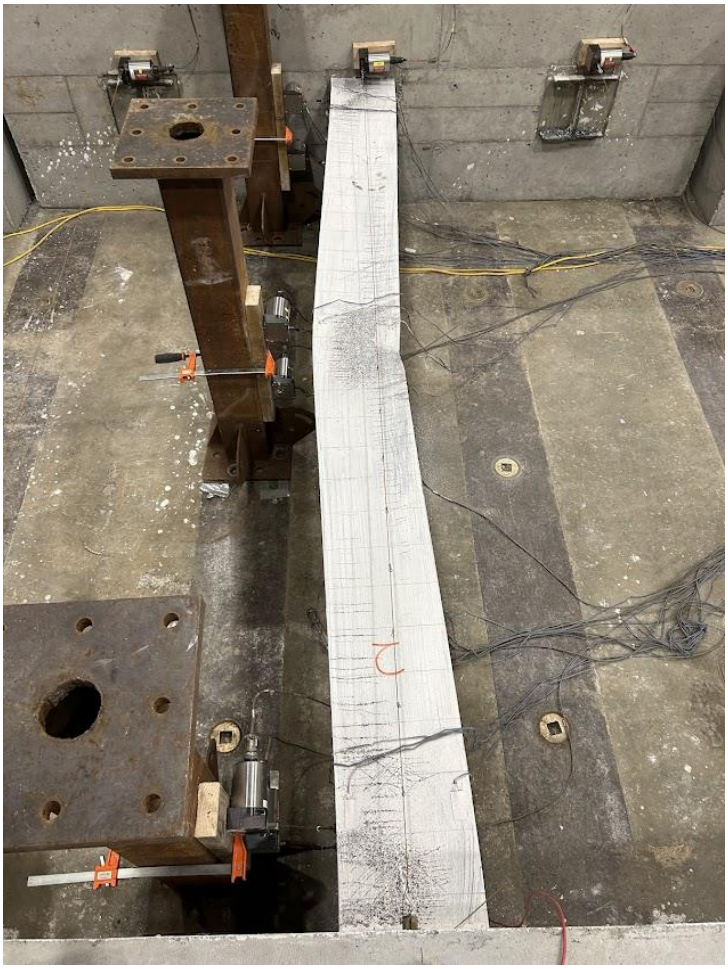

Figure 3-41. Top view of pile after completion of testing

Figure 3-42. Web and flange views of pile at sections Middle, H, and Fix after testing

4 ANALYTICAL SIMULATION FOR THE CAPACITY ESTIMATION

In previous research (Deng et al. 2018), an FE modeling method was used to calculate the capacities of individually encased piles subject to scour. This method effectively calculated capacity when the concrete encasement was included in the evaluation. The results from Deng et al. (2018) were validated through analysis and laboratory tests, and the approach can be used to help calculate pile capacities directly for full encasements.

Similar to the work in Deng et al. (2018), FE modeling was used in the present study to investigate the ultimate capacities and failure modes of fully encased piles. Since it is desired to estimate the capacities of individual piles for the sake of bridge design and load rating, the final estimated pile capacities were developed based on a single-pile model. In order to validate the results from the single-pile model and correlate them with fully encased multiple-pile construction on real bridge structures, an intermediate FE model, the three-pile model, was developed and validated against the laboratory test results presented in Chapter 3.

The purpose of the three-pile model was to validate the FE modeling approach. A model replicating the laboratory-tested assembly was developed and subjected to axial loading with a slight eccentricity to simulate geometric imperfections in the pile. The modeling details and the validation results are presented in Section 4.1.

Once the modeling approach was validated, single-pile models were developed. Hundreds of single-pile models with combinations of different pile orientations, pile section sizes, concrete encasements, and pile exposure lengths were created and analyzed. The capacities resulting from each combination are presented in Section 4.2.

4.1 Three-Pile FE Model

The three-pile FE model was developed to reflect the laboratory assembly and more closely resemble the multiple-pile configuration of in-service bridge piers than the single-pile model from Deng et al. (2018). The analytical results obtained from the three-pile model were compared to the laboratory-collected data from the single-point loading test to validate the modeling approach.

4.1.1 Model Development

The three-pile model was developed with the piles' weak axes restrained by the concrete encasement (WR). The model included three 30 ft long HP10×42 piles and a 20 ft long full concrete encasement. To mimic the boundary and loading conditions of the single-point loaded laboratory assembly, roller supports were provided along the edge of the concrete encasement, and the loading, P_{WR}, was applied at the middle pile.

Two geometric configurations were investigated. The first had a 1 ft 4 in. concrete encasement thickness that mimics the dimensions from the P10L standard and represents a worst-case

scenario for out-of-plane concrete stiffness. The second had a concrete encasement thickness of 1 ft 10 in., which is the minimum thickness for HP10 piles constructed in Iowa, and replicates the thickness of the laboratory assembly. The 3 ft pile spacing used was based on typical Iowa design standards for pile bents with steel H-piles and replicates the assembly tested in the laboratory. The width of the concrete encasement was 7 ft 10 in. The model configurations are shown in Figure 4-1 and Figure 4-2.

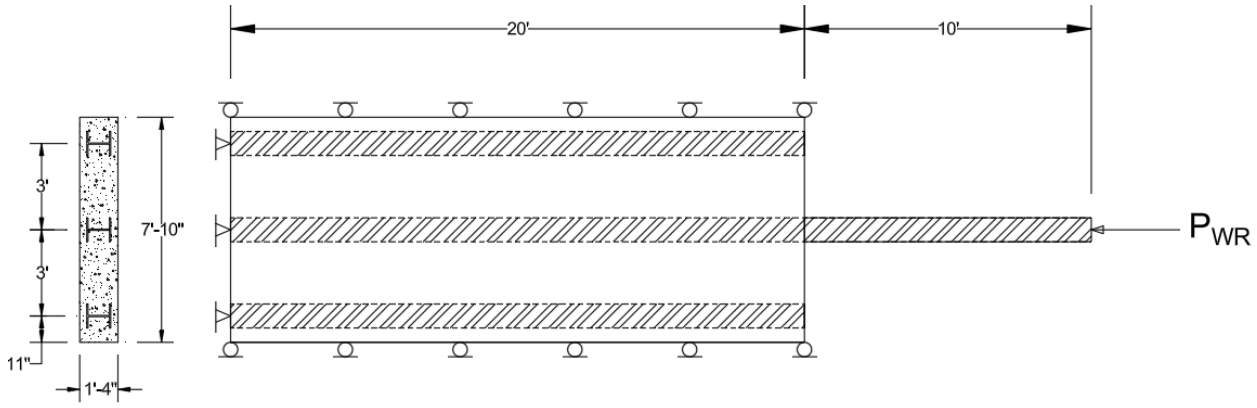

Figure 4-1. Single-pile loaded three-pile model configuration 1

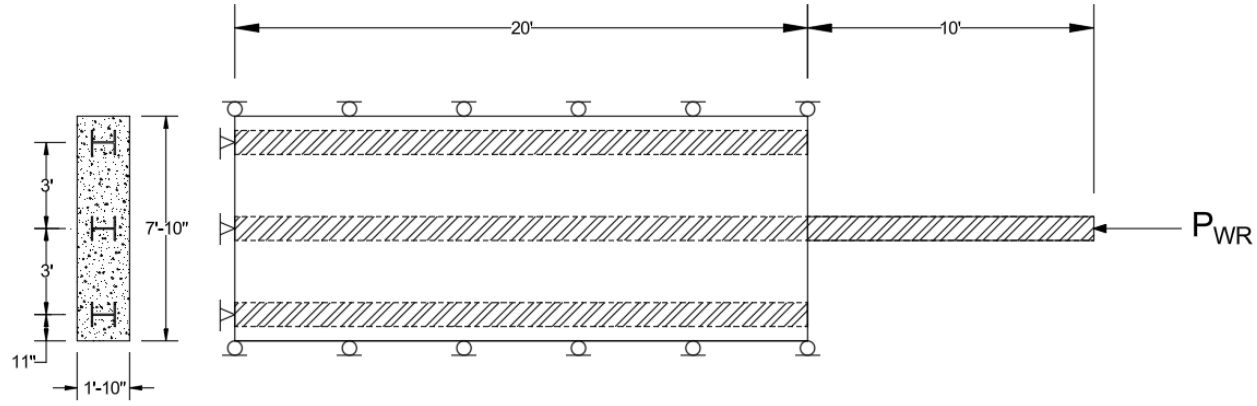

Figure 4-2. Single-pile loaded three-pile model configuration 2

The three-pile models were developed using the same approach as that used in Deng et al. (2018). The flanges and web of the steel column were both modeled using a four-node shell element with three translational and three rotational degrees of freedom at each node. The concrete was modeled using three-dimensional (3D) eight-node solid elements, which have three translational degrees of freedom at each node. The concrete element was connected to the steel H-pile through common nodes. Figure 4-3 shows the FE model for the three-pile model.

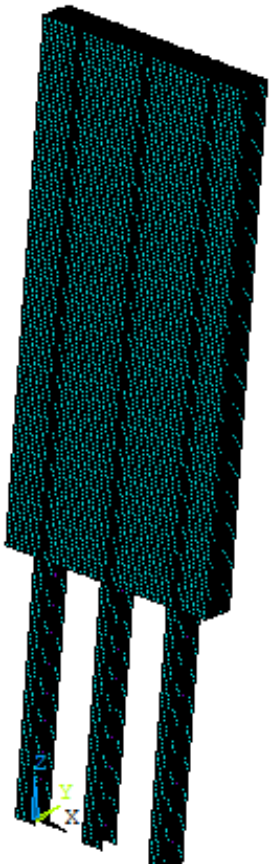

Figure 4-3. Three-pile FE model

For each model, a linear buckling analysis was performed to derive the theoretical buckling strength of an ideal column (and the bifurcation point) and provide the initial deformed shape under buckling failure. Geometric imperfections and residual stress were incorporated into the FE models. Further, the pile steel and concrete encasement were assigned nonlinear material properties to obtain the actual strengths of the piles.

The linear buckling analysis was performed with an elastic material model for the steel and concrete. The elastic modulus and Poisson's ratio of the steel were set to 29,000 ksi and 0.3, respectively. For the concrete encasement, an elastic uniaxial material model was used for the concrete, and its elastic modulus was calculated by the following:

$$E_c = 33{,}000\ x\ w_c\ x\ \sqrt{f'_c}\ \text{(ksi)}$$

where w_c = unit weight of concrete (kcf). The Poisson's ratio was set as 0.3. A compression force of 1 kip was applied to the top of the column. Pinned and fixed boundary conditions were assigned at the top and bottom of the FE model, respectively. Prestress effects were activated to calculate the stress stiffness matrix used to derive the eigenvalues of the structure under an applied loading condition. The eigenvalues are also referred to as buckling load factors, and each eigenvalue is associated with a different buckling mode. Commonly, the lowest load factor is of

interest. The estimated buckling load is derived from the product of the load factor of interest (commonly the lowest load factor) and the applied compression force. For example, if the lowest load factor is 506, the flexural buckling strength is 506 kips (i.e., the product of 506 and 1 kip).

The effects of geometric imperfections are simulated in the FE model by introducing a slight eccentricity, which also activates the inelastic buckling mode. Per Salmon and Johnson (1996), who compiled statistical data from measurements of real columns, the initial out-of-straightness of real columns ranges from $L/2000$ to $L/1000$. And per the AISC *Steel Construction Manual* (AISC 2017), the AISC equations were developed based on an initial out-of-straightness of $L/1470$. Because the AISC equations were utilized to validate the FE models, an initial out-of-straightness of $L/1470$ was used for the FE models. Geometric imperfection does not include cases where a battered pile is suspected of having non-axial loads applied (with or without eccentricities). To keep consistent with the previous research, the initial out-of-straightness of $L/1470$ was applied via an eccentric load (with an eccentricity of $L/1470$) at the top of the pile.

Residual stresses are induced in steel members during the process by which steel blanks are formed into a steel section (Salmon and Johnson 1996). The residual stresses associated with plastic deformation are caused by several factors: uneven cooling, cold bending, punching and cutting operations, and welding. For hot-rolled sections, the flanges cool more slowly than the web region, and the flange tips exposed to the air cool more rapidly than the junction between the flanges and the web. Accordingly, compressive residual stresses exist at the flange tips and the mid-depth of the web, while tensile residual stresses exist in the junction between the flanges and the web (Salmon and Johnson 1996). Abambres and Quach (2016) conducted a comprehensive literature review on research related to residual stress distribution in steel members. For bisymmetric I and H sections, residual stress has been measured by many researchers (e.g., Huber 1956, Beedle and Tall 1960, Alpsten 1968). A bilinear residual stress distribution in flanges and a symmetric distribution along the web for hot-rolled I and H sections were proposed by Galambos and Ketter (1959). A parabolic residual stress distribution in the flanges and web for hot-rolled I and H sections was proposed by Young (1972). A bilinear residual stress distribution in the flanges and web for hot-rolled I and H sections was adopted by the European Convention for Constructional Steelwork (ECCS 1984) and in the Swedish design code (BSK 99 [Boverket 2003]). To keep consistent with the previous research, a bilinear residual stress distribution was used for both the flanges and the web, as shown in Figure 4-4 (where f_y is the material yield stress and α is 0.3, which is negative in compression). The maximum residual stress is 15 ksi. The desired bilinear residual stress distribution from -15 to 15 ksi (negative in compression) was generated in the flanges and the web.

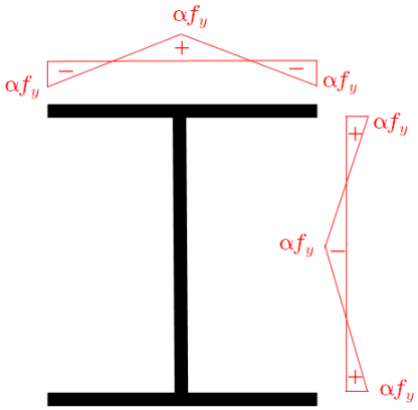

Figure 4-4. Bilinear residual stress distribution

A nonlinear buckling analysis was performed by gradually increasing the applied loads until reaching a load level at which the structure became unstable. A perfect elastic-plastic material model was used for the steel. The elastic modulus, strain hardening modulus, and Poisson's ratio of the steel were set to 29,000 ksi, 0, and 0.3, respectively. The command "Initial State" was utilized to apply the residual stress to the FE model. Note that the term "Initial State" refers to the state of a structure at the start of an analysis when the structure has not been deformed and stressed (ANSYS 2012). The concrete material properties were assigned using multi-linear isotropic hardening in combination with the von Mises yield criterion. The stress-strain relationship of concrete proposed by Hognestad (1951) was utilized for the concrete constitutive model:

$$f_c = f'_c \left[2 \left(\frac{\varepsilon}{\varepsilon_{oo}} \right) \left(\frac{\varepsilon}{\varepsilon_0} \right)^2 \right]$$

where f_c and ε are stress and strain on concrete, respectively, and strain at peak stress (ε_o) is expressed as follows (Wee et al. 1996):

$$\varepsilon_0 = 0.00126 (f'_c)^{1/4}$$

The smeared fixed crack model and Rankine maximum stress criterion were utilized to determine the initiation and development of concrete cracking. According to the AASHTO LRFD specifications (AASHTO 2015), the maximum concrete tensile strength can be derived from the following:

$$f'_t = 0.24 \sqrt{f'_c}$$

4.1.2 Model Validation against Laboratory Test Results

The resulting maximum capacity for the three-pile model in configuration 1 and the three-pile model in configuration 2 were similar because the unencased portion of the pile controlled the

ultimate capacity. This failure mode is graphically depicted in Figure 4-5, which shows the exaggerated deformed shape of the three-pile model.

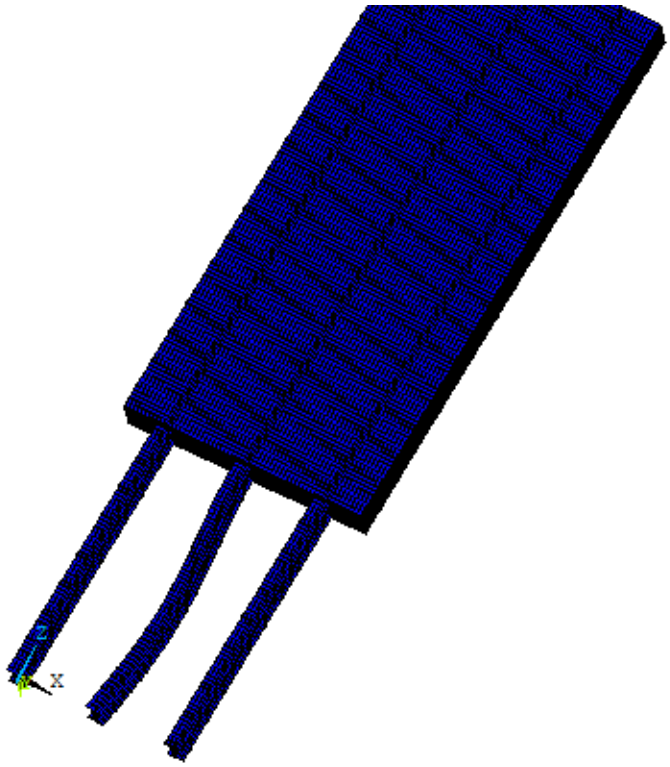

Figure 4-5. Exaggerated deformed shape of three-pile model

The analytical model estimates an ultimate capacity slightly lower than that of the laboratory-tested assembly, which may be due to the actual steel yield strength and concrete compressive strength being higher than the specified values. However, this also indicates that the analytical estimation is conservative.

The strain data collected on the steel pile at the Middle section and H section and the displacement data collected at the H section were used to validate the model. Figure 4-6 (a) and Figure 4-6 (b) compare the strain data extracted from the FE models and obtained from the laboratory test (denoted as "2" in the plots) for the Middle section and the H section; each FE model encasement thickness configuration produced the same results because the unencased portion controlled the final capacity. As the load increased, the strain behavior from the FE model and the laboratory test showed good agreement, with the laboratory test reaching only a slightly higher maximum capacity.

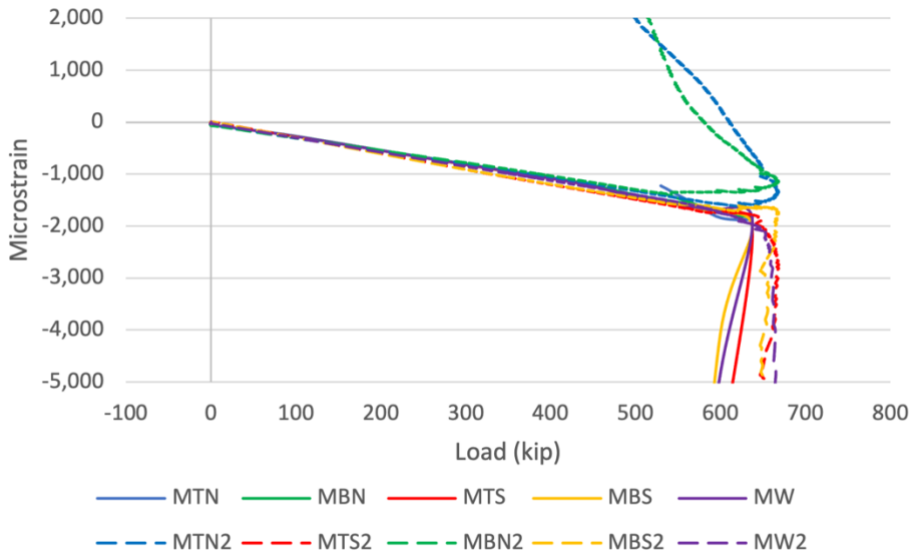

(a) Validation of model at Middle Section

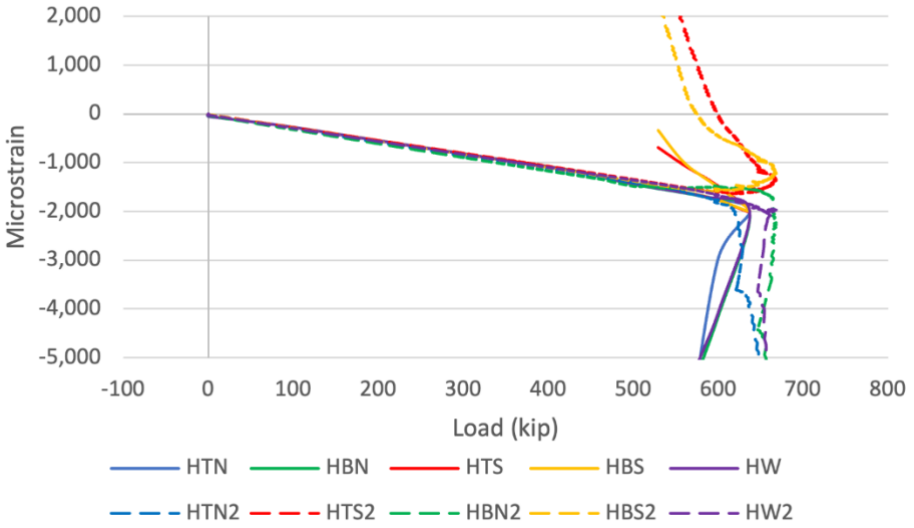

(b) Validation of model at Middle Section and H Section

Figure 4-6. Model validation comparing strain data

Figure 4-7 compares the horizontal displacement data at the H section from the FE model and obtained from the laboratory test. Similar to the strain data, the displacement data collected from the FE model and laboratory test show good agreement, except that the FE model shows a slightly lower capacity than the laboratory test assembly. These results confirm the validity of the modeling approach and support its use for further analysis.

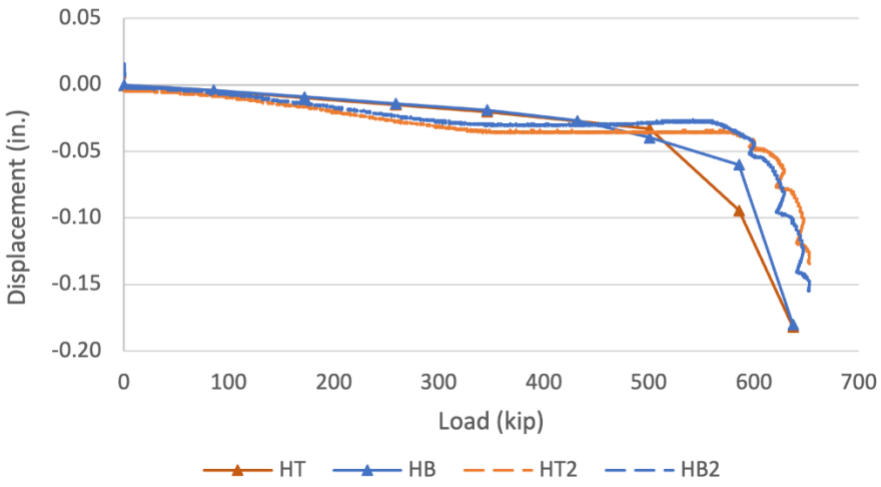

Figure 4-7. Model validation comparing horizontal displacements at H section

To design or load rate steel H-piles in Iowa, the compression load is assumed to have a 2 in. eccentricity along both axes at the top of a pile. Therefore, using the same model, the load eccentricity was modified to consider both geometric imperfection (out-of-straightness) and a 2 in. deviation in both the piles' strong and weak axes. The load was applied through displacement control with an eccentricity equal to the sum of the out-of-straightness and 2 in. The load was gradually increased until buckling failure of the pile occurred. Note that for these analyses, large deflection effects were included, stress stiffness effects were activated, and automatic load stepping was used during the nonlinear analysis. Convergence criteria and tolerances were set for the displacement, force, and moment.

A comparison of the results from the FE model with and without the additional 2 in. eccentricity is shown in Figure 4-8 and Figure 4-9. The results indicate consistent strain behavior, though the final capacity is decreased by approximately 8% to 10% when compared to the FE model without added eccentricity.

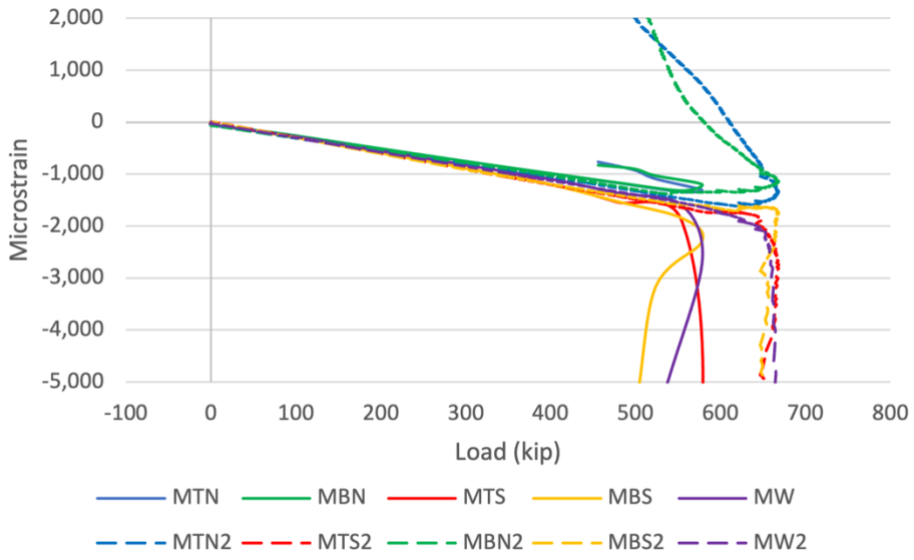

(a) Model at Middle section with an additional 2 in. eccentricity

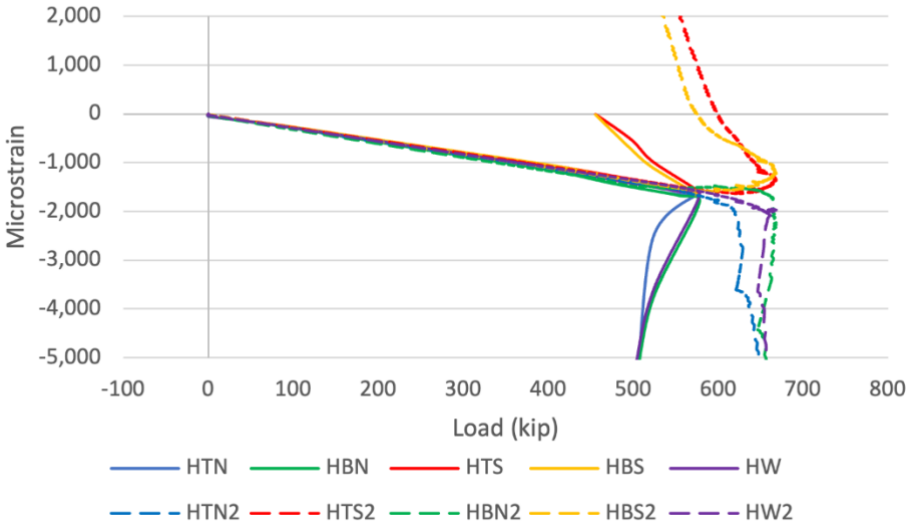

(b) Model at Middle section and H section with an additional 2 in. eccentricity

Figure 4-8. Comparison of laboratory results to FE model with an additional 2 in. load eccentricity

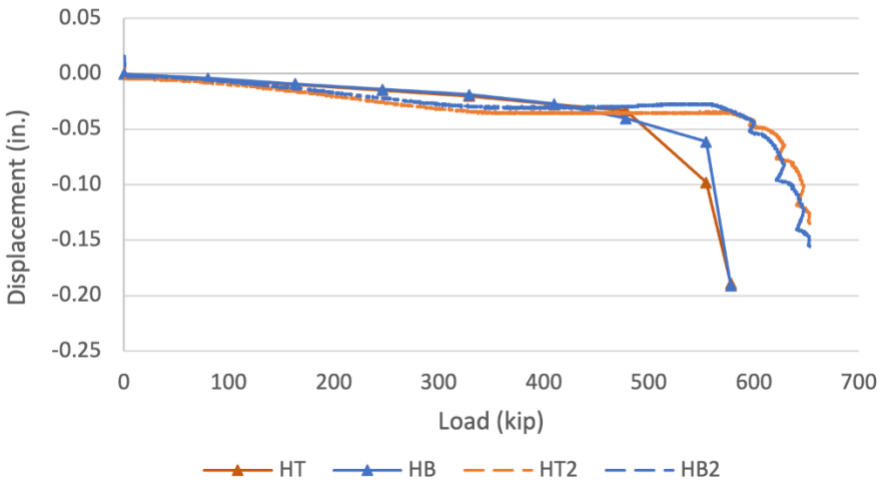

Figure 4-9. Comparison of horizontal displacements at H section with an additional 2 in. load eccentricity

4.2 Single-Pile FE Model

4.2.1 Model Development and Validation

Analysis of single piles is preferred for design and load rating. Accordingly, a simplified model consisting of only a single pile was developed based on the modeling approach used for the three-pile model, with the goal of simulating a three-pile assembly.

Recognizing that the thickness of the pile encasement does not control the ultimate capacity, the single-pile model consisted of a pile with a concrete encasement cross-section based on Iowa DOT Standard P10L, with a concrete encasement cross-section consistent with the pile size. Figure 4-10 shows a schematic view of a single-pile model with a 30 ft long pile and a 20 ft long concrete encasement, with the weak (upper schematic) and strong (lower schematic) axes restrained. To account for the lateral support from the adjacent piles and concrete, roller supports were assigned along the length of the concrete encasement. For example, the concrete encasement in the upper schematic of Figure 4-10 was restrained in the weak axis of the pile, and the concrete encasement in the lower schematic was restrained in the pile's strong axis.

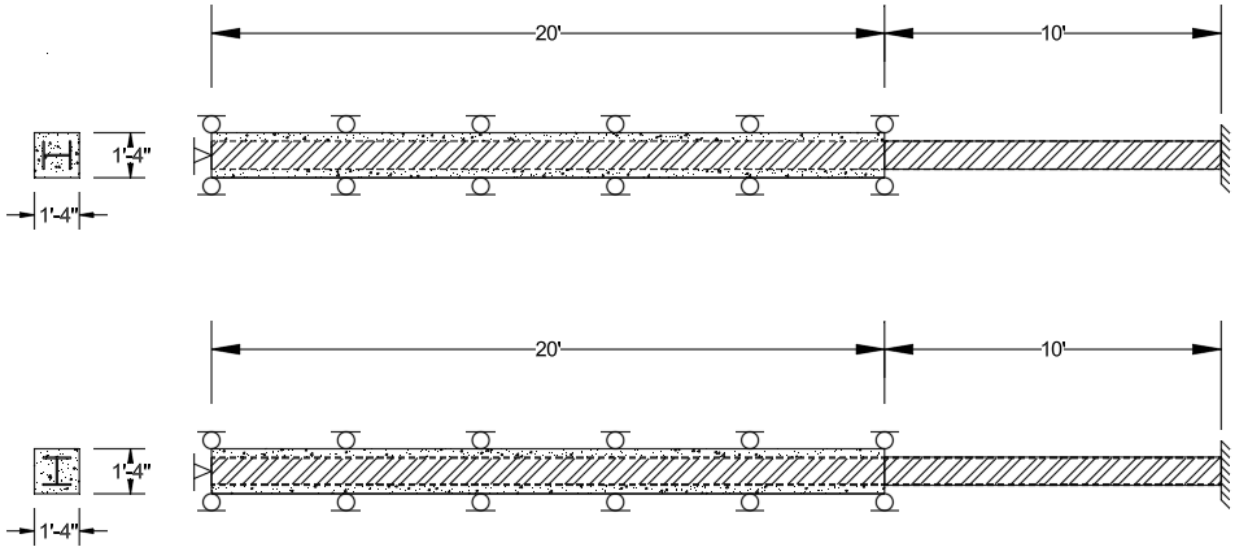

Figure 4-10. Schematic view of single-pile model with the weak axis restrained (top) and strong axis restrained (bottom)

As with the three-pile model, a linear buckling analysis was first performed on the single-pile model to derive the theoretical buckling strength of an ideal column (and the bifurcation point) and provide the initial deformed shape under buckling failure. Geometric imperfections and residual stress were incorporated into the FE model (see Figure 4-11). Like the second configuration of the three-pile model, the load was applied eccentrically in both directions at a distance of $L/1470$ plus 2 in. from the center of the pile. Further, the pile steel and concrete encasement were assigned nonlinear material properties to obtain the actual strengths of the piles with or without concrete encasements. The detailed modeling approach is presented in Section 4.1.1.

Figure 4-11. Single-pile FE model

To validate the single-pile model, the results of the single-pile and three-pile models with the weak axis restrained were compared. The single-pile model's ultimate capacity reached 575 kips, which is close to the ultimate capacity of 578 kips obtained from the three-pile model when the middle pile was loaded.

The capacity estimation results from the single-pile model are reasonably close but slightly lower than those from the three-pile model, indicating that the results from the single-pile model are slightly more conservative and that the modeling approach is valid for use in subsequent analysis.

4.2.2 Parametric Study Based on Single-Pile Model

To cover the commonly used pile design ranges, hundreds of single-pile models were developed with combinations of different pile section sizes, concrete encasements, and pile exposure lengths. In this work, five commonly used Iowa DOT pile cross-sections were modeled, including HP10×42, HP10×57, HP12×53, HP14×73, and HP14×79. For the HP10×42, HP10×57, and HP12×53 pile cross-sections, three pile lengths were included: 20 ft, 30 ft, and 40 ft. For the HP14×73 and HP14×79 pile cross-sections, two more pile lengths were included: 50 ft and 60 ft. The modeling approach used to generate the models was the same as that introduced in Section 4.2.1. The piles were modeled in two configurations: weak axis restrained and strong axis

restrained, as illustrated in Figure 4-12 and Figure 4-13. The load was applied through displacement control with an eccentricity equal to the sum of the out-of-straightness and 2 in. deviations in the piles' strong and weak axes.

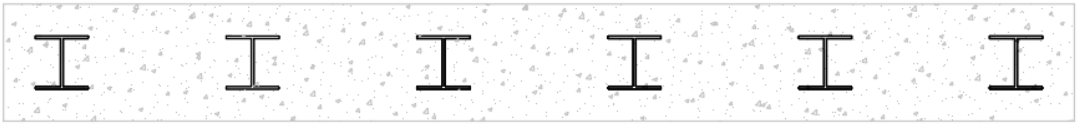

Figure 4-12. Fully encased piles with the piles' weak axes restrained

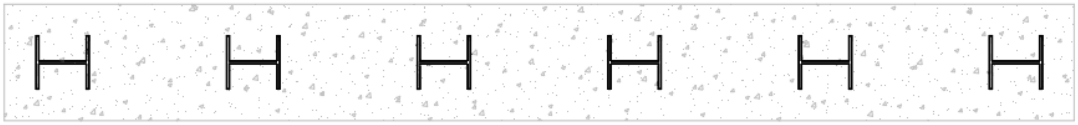

Figure 4-13. Fully encased piles with the piles' strong axes restrained

Figure 4-14 illustrates and defines the encasement length and pile length as they pertain to the models, and Table 5 presents the model variations.

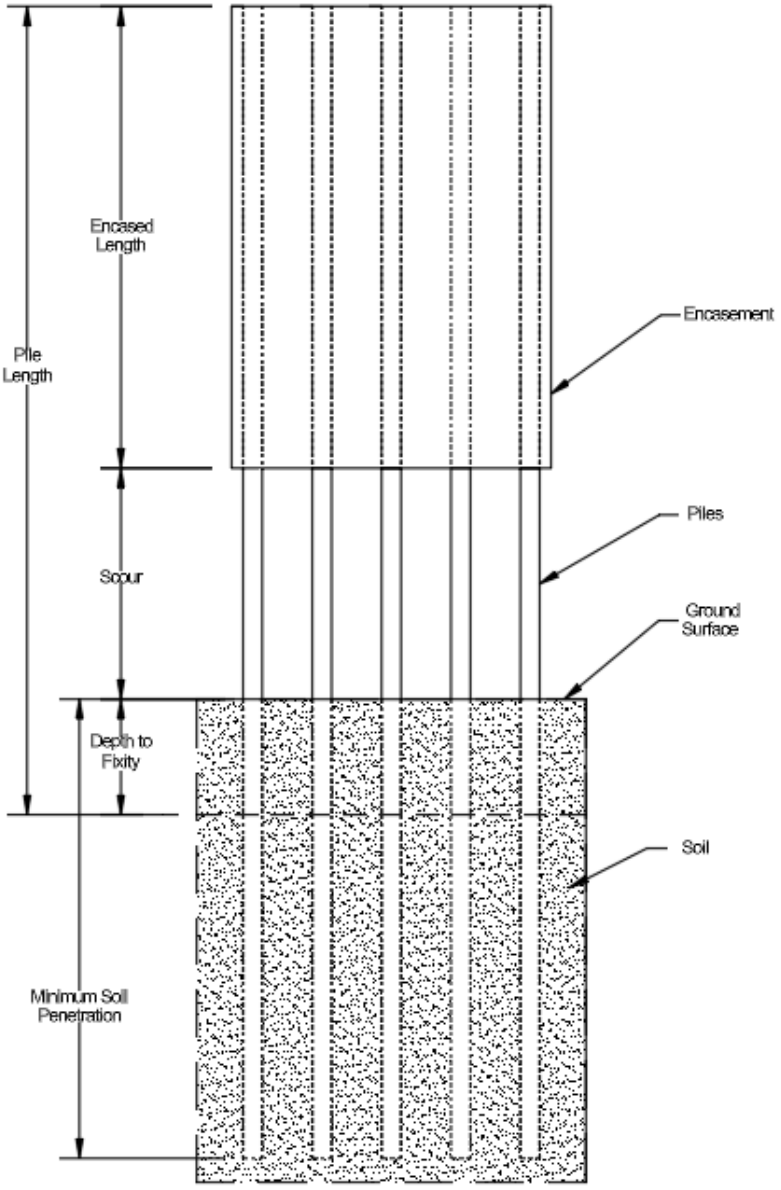

Figure 4-14. Schematic of pile bent

Table 5. Model development combinations

HP10x42		HP10x57		HP12x53		HP14x73		HP14x89	
Pile Length (ft)	**Encasement Length (ft)**	**Pile Length (ft)**	**Encasement Length (ft)**	**Pile Length (ft)**	**Encasement Length (ft)**	**Pile Length (ft)**	**Encasement Length (ft)**	**Pile Length (ft)**	**Encasement Length (ft)**
20	0	20	0	20	0	20	0	20	0
	5		5		5		5		5
	10		10		10		10		10
	15		15		15		15		15
30	0	30	0	30	0	30	0	30	0
	5		5		5		5		5
	10		10		10		10		10
	15		15		15		15		15
	25		25		25		25		25
40	0	40	0	40	0	40	0	40	0
	5		5		5		5		5
	10		10		10		10		10
	15		15		15		15		15
	25		25		25		25		25
	35		35		35		35		35
						50	0	50	0
							5		5
							10		10
							15		15
							25		25
							35		35
						60	0	60	0
							5		5
							10		10
							15		15
							25		25
							35		35

The Iowa DOT uses Structural Resistance Levels (SRLs), which are categories defined by the Iowa DOT to align with AASHTO LRFD standards. SRLs describe the structural capacity of driven steel H-piles under axial loads, incorporating factors such as material strength, load factors, and driving conditions. It is the common practice of the Iowa DOT to limit the factored load into the pile to SRL-1. SRL-1 applies a load factor (γ) of 1.45, an allowable stress of 6 ksi, and a structural resistance factor (φ_c) of 0.7 to compute factored pile capacity. Effectively, this capacity represents the structural strength of an H-pile under normal driving conditions and average soil support and aligns with past practice under Allowable Stress Design methods. A more refined analysis supporting a higher capacity is not prohibited.

Table 6 through Table 10 provide the calculated maximum axial capacities from the FE models with the piles' weak axes restrained (WR) and strong axes restrained (SR) for the HP10x42, HP10x57, HP12x53, HP14x73, and HP14x89 pile sizes, respectively. In these tables, there are a few instances where the SRL-1 capacity exceeds the capacities from the FE models. These instances are highlighted for clarity.

Table 6. HP10x42 capacity with strong or weak axis restrained compared to SRL-1 and section yield

	Pile Length (ft)	Pile Encasement (ft)	SR (kip)	WR (kip)	SRL-1 (kip)	Yield (kip)
HP10x42	20	0	225	275	107	620
		5	307	467		
		10	418	531		
		15	562	595		
	30	0	179	178		
		5	188	400		
		10	227	440		
		15	305	499		
		25	547	601		
	40	0	123	123		
		5	126	302		
		10	141	337		
		15	171	387		
		25	308	504		
		35	533	595		

Table 7. HP10x57 capacity with strong or weak axis restrained compared to SRL-1 and section yield

	Pile Length (ft)	Pile Encasement (ft)	SR (kip)	WR (kip)	SRL-1 (kip)	Yield (kip)
HP10x57	20	0	282	282	146	835
		5	314	468		
		10	427	541		
		15	570	602		
	30	0	184	184		
		5	194	408		
		10	233	457		
		15	313	507		
		25	576	608		
	40	0	127*	127*		
		5	131*	309		
		10	146*	352		
		15	177	395		
		25	315	510		
		35	537	608		

* Shaded cells indicate the SRL-1 load exceeds the capacity

Table 8. HP12x53 capacity with strong or weak axis restrained compared to SRL-1 and section yield

	Pile Length (ft)	Pile Encasement (ft)	SR (kip)	WR (kip)	SRL-1 (kip)	Yield (kip)
HP12x53	20	0	392	392	134	775
		5	432	592		
		10	556	663		
		15	705	723		
	30	0	268	268		
		5	281	533		
		10	333	575		
		15	433	630		
		25	703	733		
	40	0	192	192		
		5	197	436		
		10	218	474		
		15	261	538		
		25	438	647		
		35	703	730		

Table 9. HP14x73 Capacity with strong or weak axis restrained compared to SRL-1 and section yield

	Pile Length (ft)	Pile Encasement (ft)	SR (kip)	WR (kip)	SRL-1 (kip)	Yield (kip)
HP14x73	20	0	561	561	186	1070
		5	606	745		
		10	721	812		
		15	841	869		
	30	0	424	424		
		5	442	682		
		10	510	730		
		15	624	772		
		25	841	855		
	40	0	320	320		
		5	328	532		
		10	359	593		
		15	419	663		
		25	635	753		
		35	856	843		
	50	0	240	240		
		5	246	413		
		10	261	453		
		15	292	502		
		25	415	623		
		35	635	775		
	60	0	196	196		
		5	198	347		
		10	206	374		
		15	221	407		
		25	284	490		
		35	406	616		

Table 10. HP14x89 capacity with strong or weak axis restrained compared to SRL-1 and section yield

	Pile Length (ft)	Pile Encasement (ft)	SR (kip)	WR (kip)	SRL-1 (kip)	Yield (kip)
HP14x89	20	0	564	564	227	1305
		5	611	769		
		10	728	820		
		15	847	880		
	30	0	432	432		
		5	450	691		
		10	519	739		
		15	633	788		
		25	850	870		
	40	0	326	326		
		5	334	537		
		10	366	600		
		15	427	669		
		25	644	766		
		35	862	856		
	50	0	246	246		
		5	251	418		
		10	267	458		
		15	299	507		
		25	422	628		
		35	643	781		
	60	0	200*	200*		
		5	202*	351		
		10	210*	379		
		15	226*	412		
		25	290	495		
		35	413	626		

* Shaded cells indicate the SRL-1 load exceeds the capacity

Figure 4-15 and Figure 4-16 plot the data from these tables and graphically depict the maximum axial capacity for cases where the strong axis is restrained and the weak axis is restrained. Each graph includes a horizontal dashed line corresponding to the factored SRL-1, which is not exceeded in design practice; if more capacity is required, either more piles are added or larger piles are used. As an additional reference, a dashed line is shown representing the capacity if full section yield (stress = 50 ksi) was achieved before another failure mode.

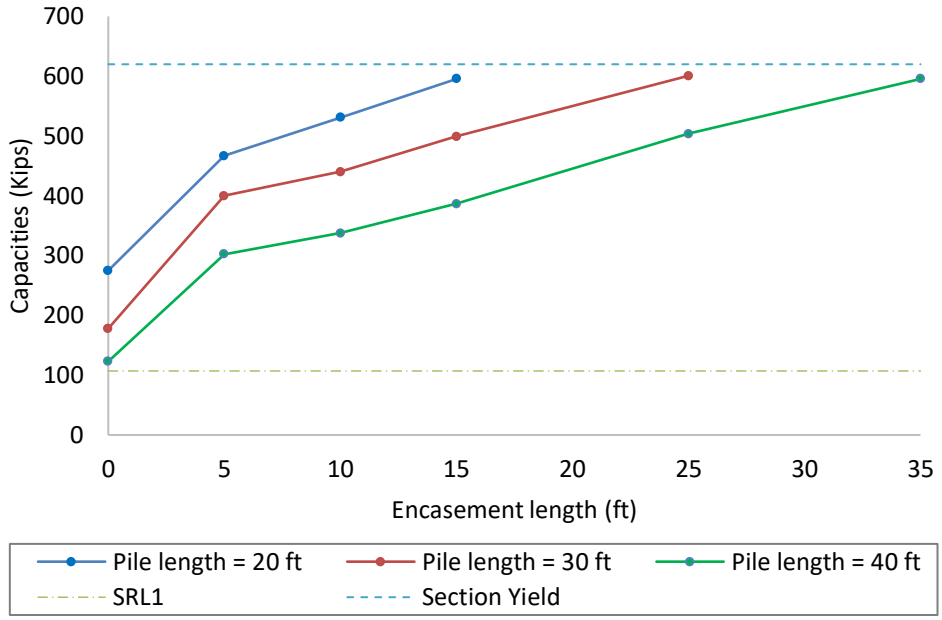

(a) HP10×42 weak axis restrained

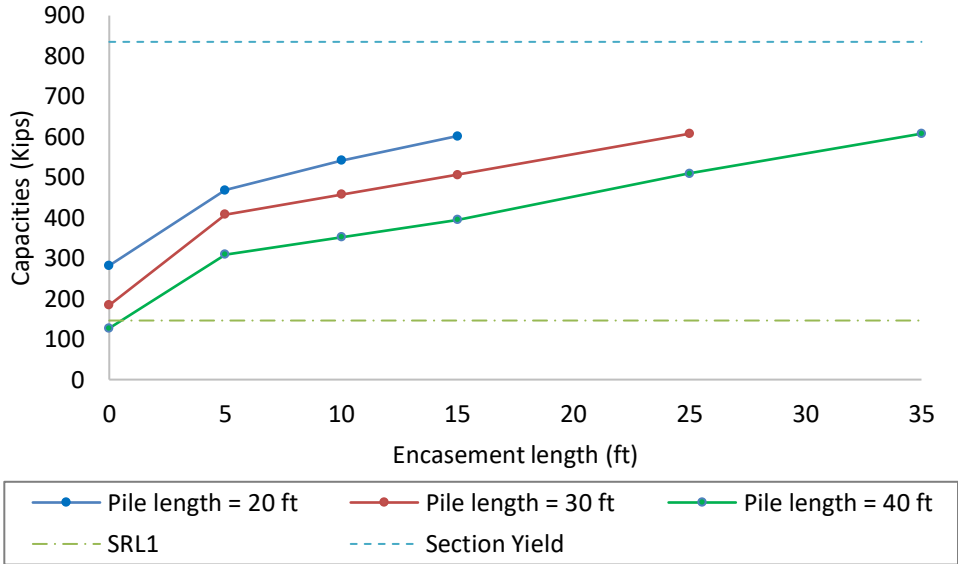

(b) HP10×57 weak axis restrained

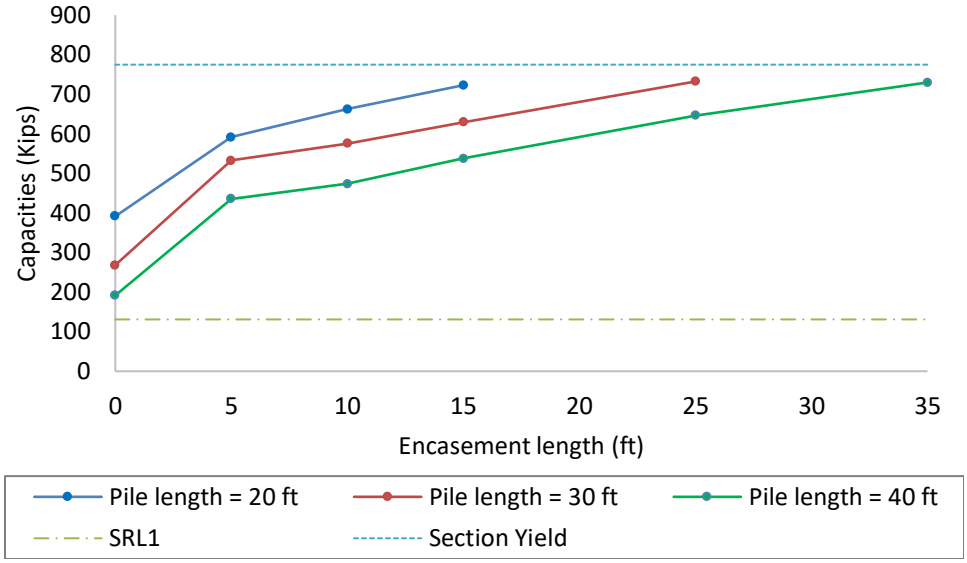

(c) HP12x53 weak axis restrained

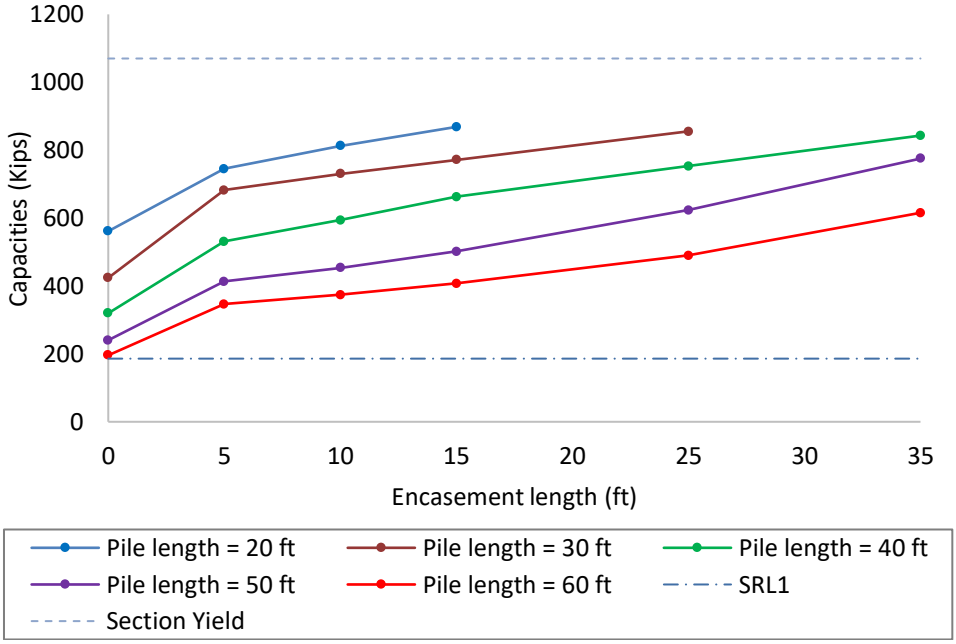

(d) HP14x73 weak axis restrained

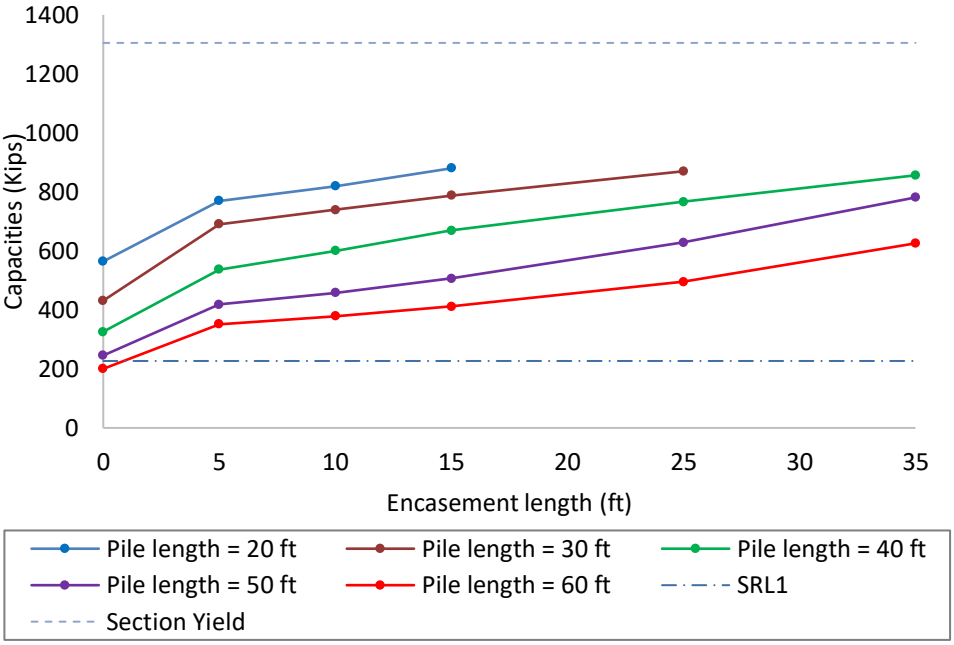

(e) HP14x89 weak axis restrained

Figure 4-15. Results for models with the weak axis restrained

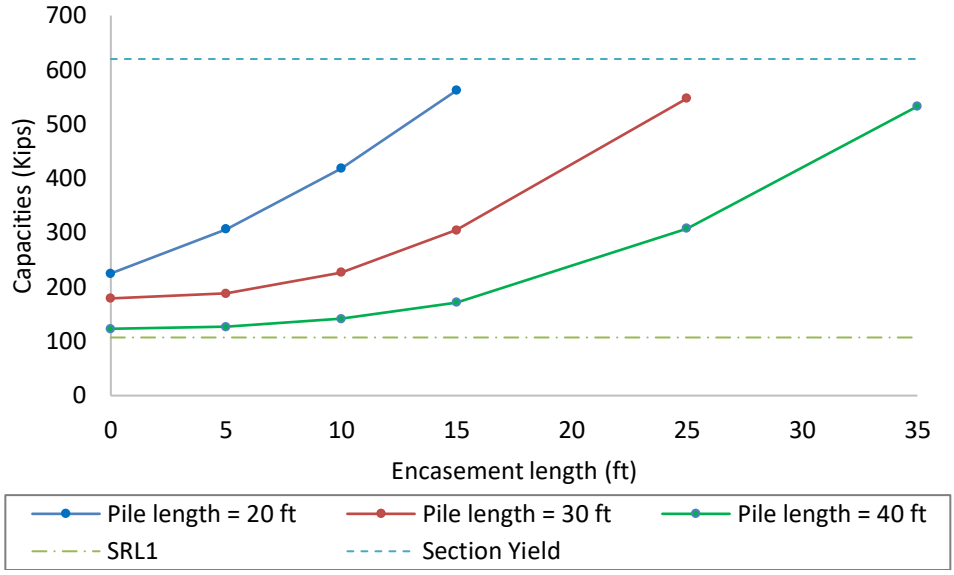

(a) HP10x42 strong axis restrained

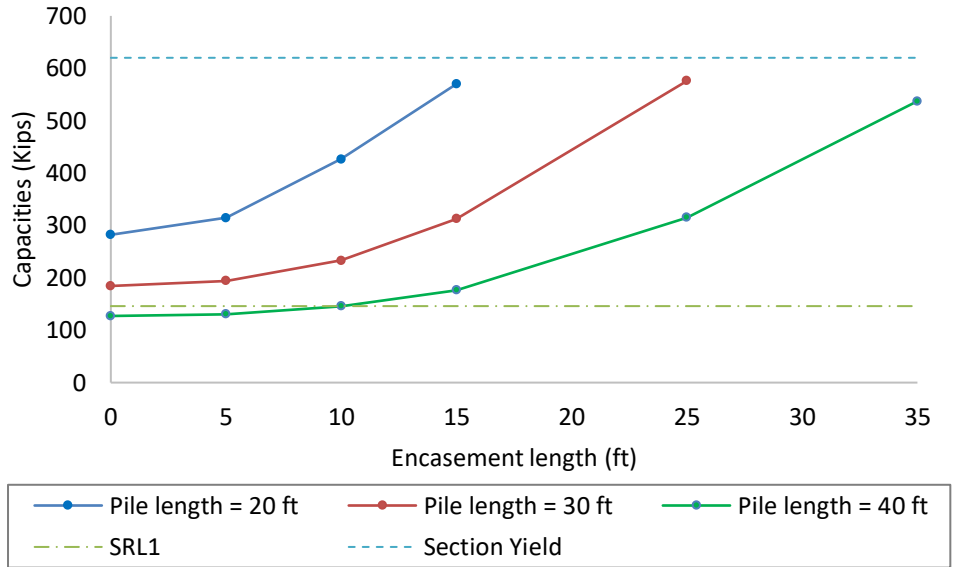

(b) HP10x57 strong axis restrained

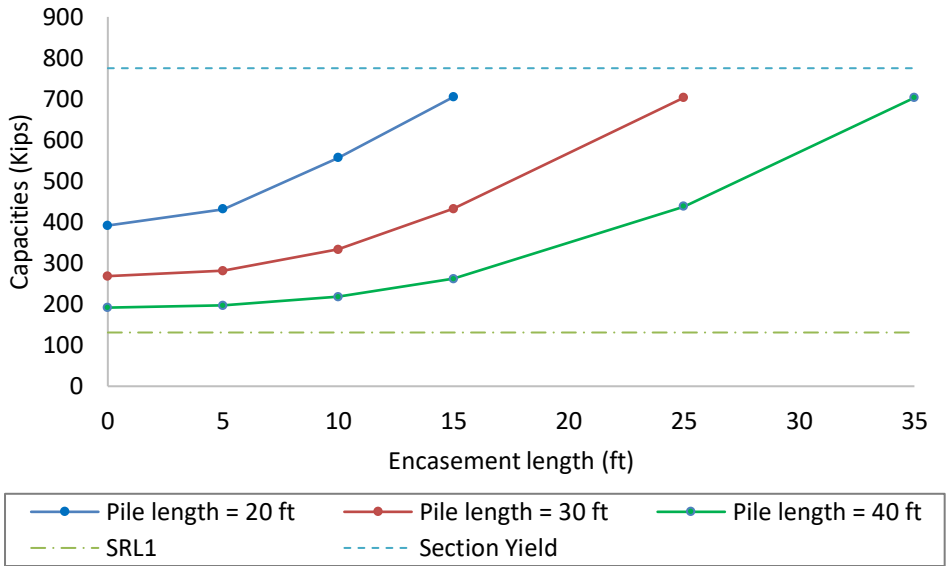

(c) HP12x53 strong axis restrained

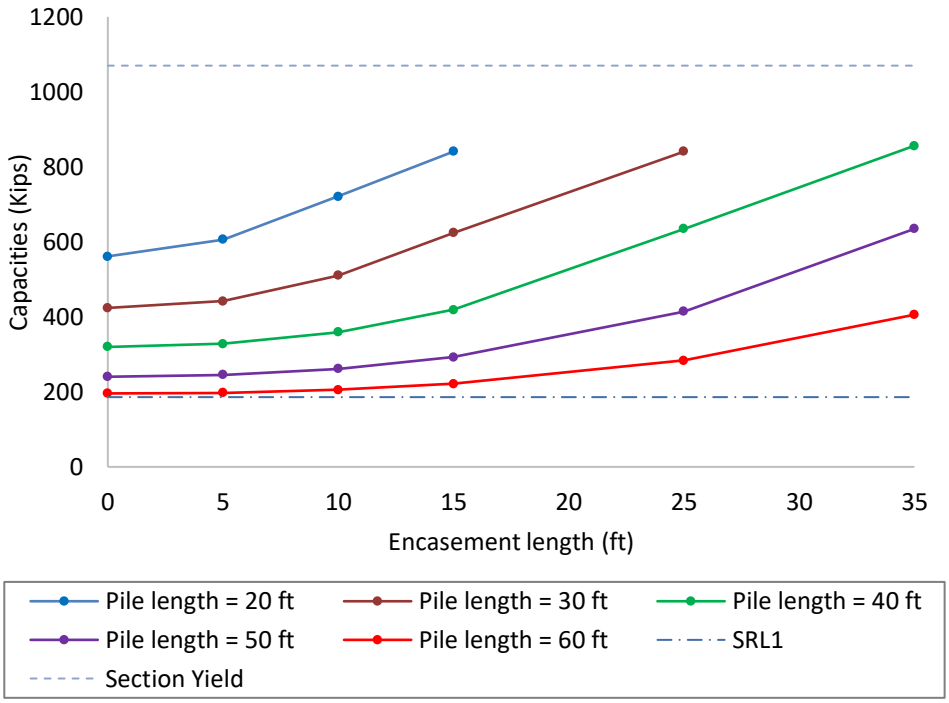

(d) HP14x73 strong axis restrained

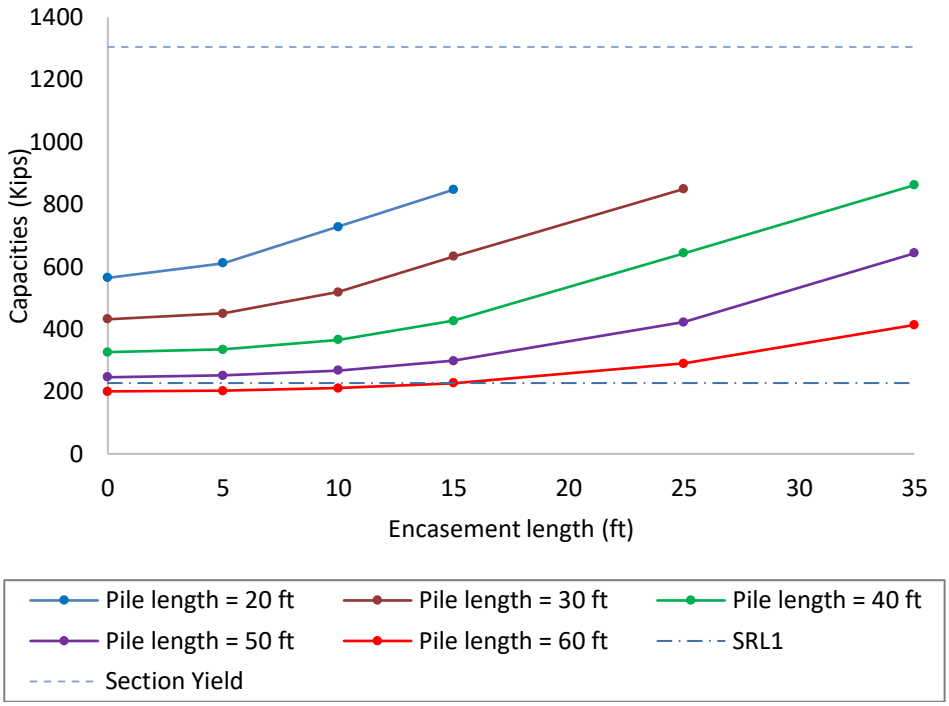

(e) HP14x89 strong axis restrained

Figure 4-16. Results for models with the strong axis restrained

The plots indicate that a longer concrete encasement results in higher ultimate capacities for piles of the same length, whether the weak axis or strong axis is restrained. Accounting for axis restraint, it can be observed that the ultimate capacities from the models with the weak axis restrained are higher than those from the models with the strong axis restrained. Furthermore, except for a few instances, the pile capacities exceed the SRL-1 load level. While the failure mode is not indicated for each case, it can be generally stated that the primary failure mode is global instability. The chances of local flange buckling increase with higher load levels.

4.2.3 Comparison with Individually Encased Piles

In this section, the analytical results obtained from Section 4.2.2 for the fully encased piles are compared with the results from the study completed by Deng et al. (2018), in which the piles were individually encased.

Table 11 presents several examples of the calculated capacities for singly encased and fully encased piles. Figure 4-17 (a) shows the comparison results for the HP10×42 piles for 20 ft and 40 ft pile lengths, and Figure 4-17 (b) shows the comparison results for the HP14×89 piles for 30 ft and 60 ft pile lengths.

Table 11. Comparison of capacities for singly and fully encased piles

Pile Type	Pile Length	Encasement Length (ft)	Singly Encased	Fully Encased	
				Weak Axis	Strong Axis
			Phase I (kips)	Restrained (kips)	Restrained (kips)
HP10x42	20 ft	0	175	225	225
		5	220	476	307
		10	380	552	418
		15	515	631	562
	40 ft	0	90	123	123
		5	110	308	126
		10	115	351	141
		15	130	410	171
		25	270	544	308
		35	480	655	533
HP14x89	30 ft	0	420	432	432
		5	520	704	450
		10	590	769	519
		15	650	835	633
		25	920	940	850
	60 ft	0	160	200	200
		5	200	358	202
		10	200	394	210
		15	200	437	226
		25	280	534	290
		35	430	688	413

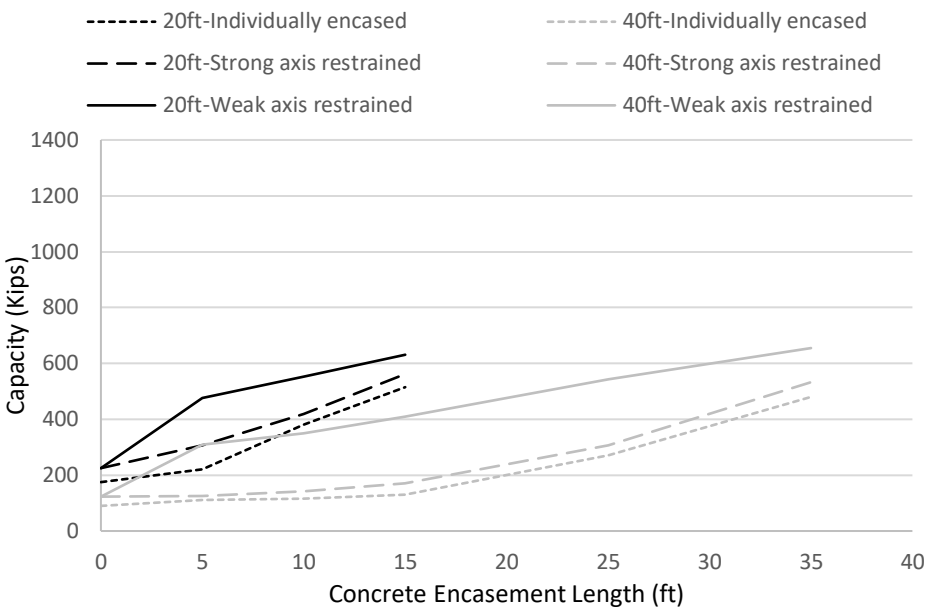

(a) HP10×42

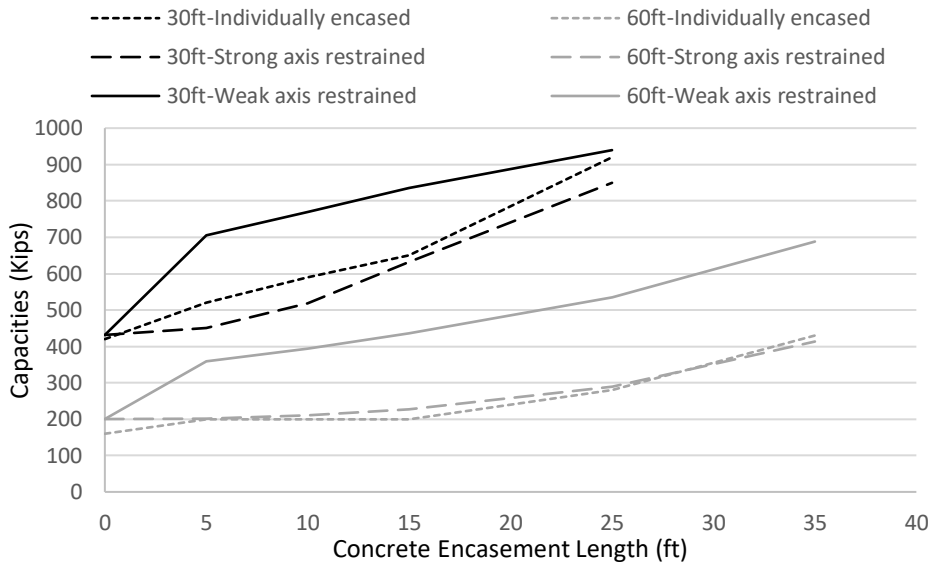

(b) HP14×89

Figure 4-17. Comparison with individually encased piles

A fully encased pile bent effectively reduces the unbraced height in the in-plane direction by the height of the concrete encasement. However, it does not provide the same benefit in the out-of-plane direction. When the strong axis is restrained, the unbraced height in the out-of-plane direction is comparable to that of an individually encased pile bent.

5 SUMMARY AND CONCLUSIONS

5.1 Overview

This study addressed the structural behavior and axial capacity of fully encased steel H-pile bents, with a particular focus on unbraced pile height in scour-prone conditions. The research was motivated by the observation that current bridge design standards, particularly in Iowa, do not consider the capacity contribution of concrete encasement, even though such encasements are widely used to protect piles from corrosion and mechanical damage. This practice has historically led to overly conservative capacity estimates and, potentially, missed opportunities for more cost-effective and resilient bridge foundation designs.

5.1.1 Objectives and Approach

The primary goal of the research was to evaluate how concrete encasement affects the axial capacity of bridge piles, especially when sections of the pile are exposed due to scour. To that end, the research aimed to do the following:

- Assess the unbraced height limits of fully encased piles.
- Expand and validate previously completed pile capacity assessment studies to include full encasement conditions.
- Compare the structural performance of fully encased piles against individually encased alternatives.
- Provide guidance for future design and load rating decisions based on experimental and analytical data.

To achieve these objectives, the research team employed a comprehensive three-pronged approach:

- **Literature Review**: Explored previous studies on concrete-encased piles, failure modes (yielding, buckling), and performance under scour conditions.
- **Experimental Testing**: Conducted full-scale laboratory tests of both a three-pile fully encased assembly and a single-pile fully encased assembly.
- **Analytical Modeling**: Developed and validated finite element models based on test data to perform parametric studies across various pile and encasement configurations.

5.1.2 Experimental Testing

Two major tests were conducted to investigate the structural behavior of encased piles:

1. **Three-Pile Assembly:** This test simulated a fully encased pile bent using three HP10×42 piles embedded in a continuous concrete encasement. The test setup was carefully constructed to simulate real-world axial loading conditions with pin-fixed boundary

conditions. Load cells, strain gauges, and displacement transducers were used to measure load distribution, stress, and deformation during axial loading. The maximum load applied was approximately 788 kips. The load distribution across the three piles remained nearly equal (34%–35%–32%), and the system remained in the elastic range throughout the loading, as evidenced by the linear stress-strain response and minimal flange displacement.

2. **Single-Pile Assembly:** The second test isolated the center pile from the three-pile specimen by removing the outer piles' unencased sections. This configuration was then loaded to failure. The pile yielded at around 620 kips and ultimately failed at 668 kips, confirming a capacity increase of about 18% over a standard P10L encased pile. Post-test inspections showed both local flange buckling and global lateral displacement, with clear indications of yielding and inelastic buckling modes.

5.1.3 Analytical Modeling

The study built upon an existing assessment tool developed in earlier work by incorporating fully encased scenarios. Laboratory data from the new tests were used to validate the modeling assumptions and results. The FE models incorporated both geometric imperfections and residual stress distributions, using material properties and boundary conditions representative of in-field bridge piers.

After validation, the single-pile models were used to conduct extensive parametric studies with variations in the following:

- Pile cross-sections (e.g., HP10×42, HP10x57, HP12×53, HP14x73, HP14×89)
- Pile lengths (20 to 60 ft)
- Encasement lengths (0 to 35 ft)
- Axis restraint directions (weak versus strong axis)

Key findings from the parametric studies demonstrated the following:

- Increased encasement length consistently improves axial capacity.
- Weak-axis restraint (i.e., orientation where concrete encasement braces the more flexible axis) significantly outperforms strong-axis restraint in terms of capacity.
- Fully encased piles consistently outperform singly encased piles across nearly all configurations, sometimes by more than 50%, depending on the axis of restraint.

The information offers bridge engineers a more accurate, efficient method for evaluating pile performance under variable encasement and scour conditions.

5.2 Conclusions

The research demonstrated that concrete encasement should be considered as a contributing structural element when evaluating the capacity and unbraced height of steel H-piles in bridge foundations. The implications of these findings are significant for both the load rating of existing bridges and the cost-effective design of new structures.

Key conclusions were as follows:

1. Concrete encasement increases capacity.

   Concrete encasement adds substantial stiffness and strength to the encased portion of the pile. Laboratory testing showed that fully encased piles exhibit axial capacities exceeding those estimated by current AISC-based calculations, which neglect the encasement. For example, the load test on a fully encased single HP10x42 pile reached a peak capacity of 668 kips, 75 kips greater than the AISC-based theoretical yield.

2. Capacity calculations provide conservative yet useful estimates.

   The updated pile capacity calculations, validated through experimental testing, yield conservative estimations (8% to 24% lower than actual test results). These conservative estimates are still significantly more accurate than traditional methods that ignore encasement. The information is suitable for both design and load rating applications, particularly in scour-affected bridges.

3. Full encasement offers system-level benefits.

   The research confirmed that fully encased pile bents behave as unified systems, distributing load evenly among piles and resisting axial loads effectively. This behavior improves structural redundancy and may reduce the risk of local pile overstress. The added stiffness from adjacent piles and continuous encasement walls enhances both capacity and durability.

4. Orientation matters: Weak-axis restraint outperforms strong-axis restraint.

   Analytical results show that orienting piles so that their weak axis is restrained by the encasement yields significantly higher axial capacity. This suggests that revising orientation practices in bridge design (i.e., rotating piles 90 degrees from standard practice) could optimize capacity and reduce material use.

5. Fully encased piles are ideal for scour-prone areas.

   In situations where scour is likely to remove surrounding soil and reduce lateral restraint, fully encased piles maintain their capacity more effectively than singly encased alternatives.

The full encasement helps limit unbraced lengths and supports higher axial loads, making it ideal for vulnerable substructures.

6. Design implications and cost savings result from the use of fully encased piles.

   With validated data, designers can confidently include encasement in their capacity calculations. This change can reduce the number of piles needed in a bent, shorten construction times, and lower costs, without compromising safety or durability.

This research provides a significant step forward in understanding and leveraging the structural benefits of concrete-encased steel piles in bridge construction. It bridges a long-standing gap between practical field design and analytical assumptions, offering validated information that improves the safety, efficiency, and economy of bridge foundations.

6 REFERENCES

AASHTO. 2015. *AASHTO LRFD Bridge Design Specifications*. 7th Edition. American Association of State Highway and Transportation Officials.

Abambres, M., and W. M. Quach. 2016. Residual stress patterns in steel members: A review. *Journal of Constructional Steel Research,* 128 (2016): 671–683.

Abdulazeez, M. M., A. Ramadan, B. Sherstha, A. Gheni, E. Gomaa, Y. Darwish, and M. A. El Gawady. 2019. *Behavior and Repair of Corroded Steel H-Piles Phase I (Axial Behavior)*. Mid-America Transportation Center.

Alpsten, G. A. 1968. Residual stresses and column strength of steel members. *Engineering Journal, AISC*, 5(2): 41–49.

ANSYS. 2012. *ANSYS Mechanical APDL Theory Reference*. Release 15.0. ANSYS, Inc.

Beedle, L. S., and L. Tall. 1960. Basic column strength. *Journal of the Structural Division, ASCE*, 86(ST7): 139–173.

Boverket. 2003. *BSK 99: Swedish Steel Construction Code*. Boverket [Swedish Board of Housing, Building and Planning].

Dawood, M., H. Karagah, C. Shi, A. Belarbi, and C. Vipulanandan. 2017. *Repair Systems for Deteriorated Bridge Piles*. Texas Department of Transportation Research and Technology Implementation Office.

Deng, Y., B. M. Phares, and P. Lu. 2018. *Development of a Rapid Assessment Tool for Pile Capacity and Stability in Response to Scour Situations*. Bridge Engineering Center, Iowa State University.

ECCS. 1984. *European Recommendations for Steel Construction*. 5th Edition. European Convention for Constructional Steelwork.

El-Barbary, A. A., M. T. Elmihilmy, and W. W. El-Tahan. 2011. Experimental tests on short composite and internally reinforced concrete columns. *International Journal of Structural Engineering*, 2(1), 35–49.

Galambos, T. V., and R. L. Ketter. 1959. *Columns under Combined Bending and Thrust*. Engineering Experiment Station Bulletin Series No. 367. University of Illinois Engineering Experiment Station.

Hannigan, P. J., G. G. Goble, G. Thendean, G. E. Likins, and F. Rausche. 1998. *Design and Construction of Driven Pile Foundations: Workshop Manual – Volume I*. FHWA-HI-97-013. Federal Highway Administration.

Hognestad, E. 1951. *A Study of Combined Bending and Axial Load in Reinforced Concrete Members*. Engineering Experiment Station Bulletin Series No. 399. University of Illinois Engineering Experiment Station.

Huber, A. W. 1956. Residual stresses and the compressive strength of steel columns. *Welding Journal*, 35(2): 65s–73s.

Hughes, D., G. E. Ramey, and M. L. Hughes. 2007. Effects of extreme scour and soil subgrade modulus on bridge pile bent buckling. *Practice Periodical on Structural Design and Construction*, 12(2): 96–108.

Iowa DOT. 2009. *LRFD Bridge Design Manual Commentary*. Iowa Department of Transportation, Bridges and Structures Bureau.

Iowa DOT. 2019. *Index of Miscellaneous Standards: LRFD Trestle Pile Bents: P10-L*. Iowa Department of Transportation, Bridges and Structures Bureau.

Iowa DOT. 2021. *LRFD Bridge Design Manual*. Iowa Department of Transportation, Bridges and Structures Bureau.
Iowa DOT. 2023. *LRFD Bridge Design Manual*. Iowa Department of Transportation, Bridges and Structures Bureau.
Kattell, J., and M. Eriksson. 1998. *Bridge Scour Evaluation: Screening, Analysis, & Countermeasures*. U.S. Department of Agriculture, San Dimas Technology and Development Center.
Khodair, Y., and A. Abdel-Mohti. 2014. Numerical analysis of pile–soil interaction under axial and lateral loads. *International Journal of Concrete Structures and Materials*, 8(3): 239–49.
Klohn, E., and G. T. Hughes. 1964. Buckling of load unsupported timber piles. *Journal of the Soil Mechanics and Foundations Division*, 90(6).
Lagasse. P. F., P. E. Clopper, L. W. Zevenbergen, and L. G. Girard. 2007. *NCHRP Report 593: Countermeasures to Protect Bridge Piers from Scour Countermeasures to Protect Bridge Piers from Scour*. National Cooperative Highway Research Program.
Liang, F., C. Bennett, R. Parsons, J. Han, and C. Lin. 2007. A literature review on behavior of scoured piles under bridges. *Contemporary Topics in In-Situ Testing, Testing, Analysis, and Reliability of Foundations*, 482–89.
Liang, F., H. Zhang, and M. Huang. 2015. Extreme scour effects on the buckling of bridge piles considering the stress history of soft clay. *Natural Hazards*, 77(2): 1143–59.
Lin, C., C. Bennett, J. Han, and R. L. Parsons. 2012. Integrated analysis of the performance of pile-supported bridges under scoured conditions. *Engineering Structures*, 36: 27–38.
Liu, X., A. Nanni, and P. F. Silva. 2005. Rehabilitation of compression steel members using FRP pipes filled with non-expansive and expansive light-weight concrete. *Advances in Structural Engineering*, 8(2): 129–41.
Liu, Z., K. S. Freeseman, B. M. Phares, and S. Mousavi. 2021a. Experimental Validation of a Rapid Assessment Tool for Pile Capacity and Stability in Response to Scour Situations. InTrans Project 19-692. Bridge Engineering Center, Iowa State University.
Liu, Z., K. S. Freeseman, J. M. Dahlberg, B. M. Phares, and M. LaViolette. 2021b. *Lateral Slide of Multi-Span Bridges: Investigation of Connections and Other Details–Phase I*. Bridge Engineering Center, Iowa State University.
McClelland, B., and J. A. Focht, Jr. 1958. Soil modulus for laterally loaded piles. *Transactions of the American Society of Civil Engineers*, 123(1): 1049–63.
MnDOT. 2023. *LRFD Bridge Design Manual*. Minnesota Department of Transportation
Mousavi, S., B. M. Phares and Z. Liu. 2022. Experimental study of full-scale bridge steel h-piles' buckling with concrete encasement. *Journal of Bridge Engineering*, 28(11).
Rahman, S., M. Begum, and R. Ahsan. 2016. Comparison between experimental and numerical studies of fully encased composite columns. *International Journal of Structural and Construction Engineering*, 10(6), 756–763.
Salmon, C. G., and J. E. Johnson.1996. *Steel Structures: Design and Behavior, Emphasizing Load and Resistance Factor Design*. 4th Edition. HarperCollins College Publishers, 1996.
Timoshenko, S., and J. M. Gere. 2009. *Theory of Elastic Stability*. Dover Publications.
Vijay, P. V., P. R. Soti, H. V. S. GangaRao, R. G. Lampo, and J. D. Clarkson. 2016. Repair and strengthening of submerged steel piles using GFRP composites. *Journal of Bridge Engineering*, 21(7), 04016038.

Vogt, N., S. Vogt, and C. Kellner. 2009. Buckling of Slender Piles in Soft Soils. *Bautechnik*, 86(S1): 98–112.
Wee, T. H., M. S. Chin, and M. A. Mansur. 1996. Stress-strain relationship of high-strength concrete in compression. *Journal of Materials in Civil Engineering*, 8(2): 70–76.
Winkler, E. 1867. Die Lehre von Elastizitat und Festigkeit (on Elasticity and Fixity).
WisDOT. 2023. *Bridge Manual*. Wisconsin Department of Transportation.
Young, B. S. 1972. The distribution of residual stress in hot-rolled structural sections. *Welding Journal Research Supplement*, 51(8): 359s–365s.

THE INSTITUTE FOR TRANSPORTATION IS THE FOCAL POINT FOR TRANSPORTATION AT IOWA STATE UNIVERSITY.

InTrans centers and programs perform transportation research and provide technology transfer services for government agencies and private companies;

InTrans contributes to Iowa State University and the College of Engineering's educational programs for transportation students and provides K–12 outreach; and

InTrans conducts local, regional, and national transportation services and continuing education programs.

IOWA STATE UNIVERSITY

Visit **InTrans.iastate.edu** for color pdfs of this and other research reports.